FORCE STUDIES OF MULTIPLE KINESIN-1 AND EG5 MOLECULAR MOTORS

BY

EVAN TACLIBON GRAVES

B.S., Rose-Hulman Institute of Technology, 2000
M.S., University of Illinois at Urbana-Champaign, 2002

DISSERTATION

Submitted in partial fulfillment of the requirements
for the degree of Doctor of Philosophy in Physics
in the Graduate College of the
University of Illinois at Urbana-Champaign, 2009

Urbana, Illinois

Doctoral Committee:

Professor Taekjip Ha, Chair
Professor Paul Selvin, Director of Research
Professor Yoshitsugu Oono
Professor Russell Giannetta

ABSTRACT

Kinesin-1 and Eg5 are molecular motors that are essential for eukaryotic cell growth and development. Kinesin-1 motors transport intracellular cargo along the microtubule cytoskeleton through and against the dense viscoelastic cytoplasm. Eg5 motors mediate proper mitotic, microtubule spindle assembly during cell division, and then stabilize these spindle structures through a balance between plus-end directed and minus-end directed forces along the filaments. Therefore, it is important to understand how multiple kinesin-1 and Eg5 motors withstand competing forces, their structural rigidity under such loads, and how quickly they are able to rebind if loosed from microtubules. Using a unique type of analysis for our optical trapping experiments, we are able to get motor binding stoichiometry inaccessible by previous techniques. With this information we characterize both motors comparing them to one another. We find that the release forces for both types of motors add linearly with the number of motors bound and that Eg5 has a weaker binding than that of kinesin-1. The stiffness for the motor domains is comparable, yet we find that the average time to rebind for Eg5 decreases at higher concentrations while it does not for kinesin-1. This may indicate that there exists some weak interaction between kinesin-1 and microtubules keeping them close while unbound.

In memory of my sister, Elena

ACKNOWLEDGEMENTS

There are numerous people whose help and support made the works presented here possible. I would like to thank my thesis adviser, Paul Selvin for his help and understanding. Enormous thanks to the members of the Selvin lab who helped educate, mentor and encourage me through the process: Jeff Riefenberger, David Posson, Tania Chakrabarty, Greg Snyder, Matt Gordon, Erdal Toprak, Ben Blehm, Tyler Lougheed, Hamza Balci, Mindy Hoffman, Hasan Yardimci, Pinghua Ge, Paul Simonson, Ahmet Yildiz, Hyokeun Park, Hyeong Jun Kim, and others. Thank you to my friends, Micah Stoutimore, Joe Altepeter, Evan Jeffrey, Kerrie Huizinga, Michelle Nahas, Amy Rieter, Carla Heitzman, Emily Klein, George Glekas, and Amy Dunlap for their support through my graduate career. Most of all, I would like to thank my brother, mother and father whose encouragement to follow my dreams helped lead me here. Additionally, I would like to thank the University of Illinois for a first year academic fellowship, the Molecular Biophysics Training Grant for two years of financial support and project funding from the NSF (DBI-0649779) and the NIH (068625).

TABLE OF CONTENTS

CHAPTER 1: INTRODUCTION 1

CHAPTER 2: MATERIALS AND METHODS 22

CHAPTER 3: RESULTS 42

CHAPTER 4: DISCUSSION 61

CHAPTER 5: CONCLUSION 65

REFERENCES 70

APPENDIX: SOFTWARE PROGRAMS 76

CURRICULUM VITAE 85

CHAPTER 1: INTRODUCTION

The work presented here will focus on measuring force dependent properties of the molecular motors kinesin-1 and Eg5. Characterization of these motors was preformed using an optical trapping assay to measure release force, stiffness constants and binding rates over varying numbers of motors engaged in cargo transport. This chapter will present background information pertinent to the kinesin-1, Eg5 and the optical trapping technique.

1.1 Molecular motors

Molecular motors are proteins that convert chemical energy into mechanical energy. Here, chemical energy takes the form of molecular bonds within small molecules. The most common molecule used for chemical energy in cellular organisms is adenosine tri-phosphate (ATP). Molecular motors power themselves by utilizing the energy gained from cleaving a chemical bond within ATP. This bond-breaking process separates ATP into adenosine di-phosphate (ADP) and a single free phosphate (Pi). Under standard cytoplasmic conditions within the a cell, this produces between 11 and 13 kcal/mole (46 – 54 kJ/mole, 0.48 – 0.56 eV/molecule, or 18 – 22 k_BT/molecule) worth of energy [1]. Molecular motors use this energy to undergo a conformational change in their structure to aid in the completion of a specific task requiring motion. Examples of these tasks include muscle contraction, intracellular transport, DNA maintenance, and cell division, etc. [1-5].

The work presented here is focused on molecular motors of the Kinesin superfamily. Kinesin proteins are integral for intracellular transport of organelles, cell

morphology [6, 7] and spindle formations and movements during cell division [8-10]. Structurally, Kinesin proteins consist of a globular region of ~360 amino acids (aa) at one end, referred to as the "head," and a long alpha-helical region (~600 aa) that extends towards the opposite end called the "tail" [11] (Fig. 1.1). The head region contains the site where ATP binds and is hydrolyzed, sometimes referred to as the "catalytic core." It also contains the region which binds to tube-like, protein polymers called microtubules [12], the tracks upon which Kinesin molecules move. Microtubules are long, rigid structures that extend out from organelles called centrosomes located near the nucleus. Microtubules are structurally asymmetric filaments with a "minus" end, from which most Kinesins move away from, and a "plus" end, which most Kinesins move towards [13].

The Kinesin superfamily is a collection of over 14 separate Kinesin families [14]. The work presented here will focus on proteins of the Kinesin-1 (previously KHC) and Kinesin-5 (previously BimC) families.

1.2 Kinesin-1 Motors

The first Kinesins to be reported are those motors belonging to the highly conserved Kinesin-1 family. Present throughout the cytoplasm of all eukaryotic cells, Kinesins of this family are responsible for organelle, vesicle and nuclear transport [15, 16]. Kinesin-1 motors exist as homodimers as the two tail regions wind around one another by means of hydrophilic interactions to create a coiled-coil structure (Fig. 1.1). At the far end of the tail regions, the C-termini of the proteins, are sites where the Kinesin-1 motors bind their cargo for transport [17]. At the N-termini are the two heads where the protein motility takes place.

This family of Kinesins process along microtubule tracks transporting cargo for extended distances to reach their destination. They move by, what has been referred to as, a "hand-over-hand" mechanism. Here, the leading head remains bound to the microtubule while the trailing head releases, swings forward past the other head, and rebinds to the microtubule ahead of the other. This results in the leading head and trailing head having exchanged order, and the motor's center of mass has traversed a distance half that of the moving head [18]. This is the same mechanism by which humans walk on their feet, with the trailing foot becoming the leading foot at every step. Each head alternatively generates the conformational changes necessary for walking by catalyzing the hydrolysis of a single ATP molecule. Each nucleotide state bound within the heads (ATP, ADP + Pi, ADP, and no nucleotide state) corresponds to a different conformation of the motor protein and a different affinity for microtubules. When a head domain contains only an ADP, the affinity for microtubules is weak and the head dissociates. In the ATP, ADP + Pi or no nucleotide state the affinity for microtubules is high and the head remains tightly coupled to the microtubule. Through successive binding, hydrolyzing and releasing of ATP between the two heads, kinesin-1 is able to process along the microtubule [19]. A diagram of this catalytic ATP cycle for Kinesin-1 stepping is shown in figure 1.2.

Kinesin-1 molecules are so ubiquitous and essential in cellular processes that they currently command great focus in biological research. Their function as transporters has captured the interest of numerous researchers and driven a large number of studies in the fields of molecular motors and single molecule biophysics. The studies preformed on

Kinesin-1 are extensive, but certainly not complete. There is still a lot of information to be garnered from the study of these motors and their stepping mechanics.

The particular protein of interest for experiments presented here comes from the human genome and goes by the same name as its family, kinesin-1. It is an intracellular transporter in cells transporting cargo throughout the cytoskeletal structure. *In vitro,* and likely *in vivo,* a single kinesin-1 is capable of transporting vesicles [20-23]. *In vivo,* multiple motors likely operate simultaneously [24, 25]. Therefore, despite the fact that force properties of single kinesin-1 have been characterized in the past [26-29], it is important to study the properties of multiple kinesin-1 motors collectively engaged in cargo transport. This is some the motivation driving the experiments preformed here. The rest stems from the molecular motor Eg5 and a comparison between the two.

1.3 Kinesin-5 Motors and Eg5

The most evolutionarily conserved family of all Kinesins is the Kinesin-5 family [14]. Kinesin-5 motors homotetramers [30]. Two protein molecules combine through a coiled-coil construction, similar to Kinesin-1 motors, and two of these dimers combine linking tail regions to form the tetramer. The fully constructed Kinesin-5 complex then has two ends, each with two heads capable of walking on microtubules (Fig . 1.1) [31]. They use this tetrameric structure to crosslink two microtubules, two heads walking on each [32].

All Kinesin-5 motors are present during cell mitosis and are localized to the spindle microtubules [31] where they aid in the formation, stabilization and elongation of those spindles [33]. During cell division, mitosis, DNA chromosome pairs must divide

evenly into the two daughter cells. To do so, they align in the middle of the cell upon a scaffolding structure constructed of microtubules. This scaffolding is called the mitotic spindle. The spindle is assembled of microtubules sprouting out of two separate poles, centrosomes, on either end of the cell. Microtubules extend from the centrosomes, like long, thin spines from a sea urchin, and meet in the center of the dividing cell. Proteins crosslink the microtubules and the bi-polar mitotic spindle is formed. Throughout the mitotic process, the chromosome pairs attach to the spindle, align along the meridian of the cell, split and separate towards the two poles, each to become part of either daughter cell [1]. Kinesin-5 motors are proteins which crosslink these microtubules, forming a proper mitotic spindle, allowing proper chromosome separation to occur (Fig. 1.3).

Eg5 is a molecular motor from this Kinesin-5 family [31]. Its main function is constructing and maintaining mitotic spindles by crosslinking parallel and anti-parallel microtubules in the formation of the mitotic spindle and separation of the centrosomes during the early stages of mitosis [32, 34, 35]. This is essential to cell reproduction as previous experiments have shown that the inhibition of Eg5 results in improper spindle formation resulting in the inability for cells to divide properly [36, 37]. For this property, Eg5 is pharmaceutically targeted by the drug Monastrol. It is used for chemotherapy treatments in cancer patients since targeting and inhibiting Eg5, cancer cells are unable to divide and multiply [38, 39]. Crosslinking lengthy microtubules requires multiple Eg5 motors to cooperatively anchor the spindles against cell structural forces and also the pull of separate oppositely-directed motors that are also present on the microtubules [9, 40, 41]. Therefore, studying the properties of multiply engaged Eg5 motors is of particular relevance and interest.

1.4 Optical Trapping

Optical traps are exceptionally useful tools for studying molecular motors. They are capable of containing and manipulating microscopic particles while simultaneously measuring displacement, velocity, and forces active upon those particles in real time [42, 43]. If an infrared laser beam is focused down to a point within an aqueous solution using a powerful lens, such as a microscope objective, translucent particles in solution are drawn to and held at this focal point of the beam. Motion of the particle away from the center of the focus can be detected by measuring the corresponding refraction of the laser through the particle. By attaching molecular motors to the particles and measuring their displacements people have been able to study the mechanical behaviors of various Kinesin proteins [20, 29, 44, 45]. In the studies presented here, Eg5 and kinesin-1 motors will be attached to polystyrene beads to be placed in an optical trap for study.

How do the optical traps work? Optical traps are able to draw translucent particles into the center of a lens-focused laser beam by taking advantage of the difference in index of refraction between the particle, a polystyrene bead for the work presented here, and the surrounding media, water. It also utilizes the spatial gradient of photons around the point where the beam is focused. The bead is composed of a dielectric material. When light, an electromagnetic oscillation, passes through a dielectric material it induces electric dipoles, $\mathbf{p}$. If the electric field varies spatially in strength then a dipole will feel a force equal to $\mathbf{p} \cdot \nabla \mathbf{E}$ corresponding to different charges feeling the strength of the field at different locations. Here the induced dipoles are within the dielectric medium, the polystyrene bead, and are proportional to the electric field

strength and the polarizability of the medium. The polarizability is $\alpha = r^3 n_w^2[(n^2 - 1)/(n^2 + 2)]$, where r is the radius of the bead, n_w is the index of refraction of water, in which the bead is submerged, and n is the index of refraction of the bead itself [46]. So, the trap force due to the gradient of the beam is given by:

$$F_{grad} = - (\alpha/2) \cdot \nabla E^2$$

which continually pulls the bead to the center of the trap until it is at the point where the field is strongest at $\nabla E = 0$ over the volume of the bead.

For particles larger that the wavelength of the trapping laser a classical ray description is also adequate for describing the trapping force. A diagram of the ray-optics depiction is presented in figure 1.4. As the photons pass through the transparent bead they are refracted, due to the difference in the index of refraction between the water and the glass, and exit the bead on a trajectory that is not collinear with the path of entry. This alteration in path corresponds to a change in the photon's momentum. Conservation of momentum dictates that the bead must incur a change of momentum in an equal and opposite direction. A continuum of these refracted photons creates a cumulative force on the bead directed towards the focus, or center of the trap. Figure 1.4.a shows a bead that is centered with respect to the left and right directions, but slightly below the center of the trap. The change in photon momentum creates a force on the bead that is up, towards the focus of the laser beam. Figure 1.4.b shows a bead that is not only below the center of the trap, but also to the right of center. Due to the peaked distribution of the beam profile there are more photons being diffracted entering on the left side and exiting on the right than vice-versa. The photon momentum change is more drastic on the left entering side, resulting in a trap force on the bead directed to the left. These forces combine to create a

net force that is always directed towards the focal point of the beam from wherever the bead lies. Therefore, if the bead is not tethered, the trapping force will reposition the bead to the trap center. There are two other forces acting on the bead. One comes from any portion of the laser beam that scatters off the bottom face of the bead and is directed back towards the incoming beam. This photon momentum change adds an upward component of force. The second is gravity since the particle is denser than the surrounding solution. However, these add very minor effects to the resting position of the bead along the axis of the trapping laser. Since measurements performed here are within the plane perpendicular to this axis, we will not have to consider these last two forces.

Under the Gaussian cross-sectional profile of the trapping laser profile movements of the bead out from the trap's center results in a restoring force exerted by the trap that may be accurately modeled as a linear spring if the displacements are significantly small. More plainly put, a bead displaced from the trap's focus by a vector $\mathbf{d}_t$ will feel a force of $\mathbf{F}_{trap} = -\kappa\mathbf{d}_t$ back towards the focus. Here κ is the spring constant of the trap, determined experimentally from calibration techniques described later. This is generally true for displacements within the two-dimensional focal plane of the focusing lens of the trap. We will refer to this in the future as the x-y-plane. This linear modeling is also possible for small displacements away from the focus along the beam path, the z-direction, but with a significantly different stiffness, or spring constant, than that of the x-y-plane. Since all of the measurements pertinent to the work here are contained within the x-y-plane, all future references to movement, forces and trap stiffness will be assumed to be within that plane as well unless otherwise stated.

When the bead is displaced from the center of the trap, not only does the beam affect the bead, but the bead also affects the beam. The curvature of the spherical bead and the difference in index of refraction between it and the surrounding water create a lensing effect on the laser path. When the bead is off to one side of the center, the trajectory of the beam's centroid is angled in that direction. Therefore, in the trap's focal plane, positional changes of the bead translate into angular changes of the beam's trajectory. By taking advantage of this effect on the trapping laser light, one can determine how far the bead is from the center of the trap. We must first be able to measure this positional displacement, $\mathbf{d}_t$, in order to determine the magnitude and direction of the force applied to the bead from the trap.

To acquire this distance we take advantage of back focal plane imaging. When imaging with one lens, the object to be imaged is in the "sample plane" and the image produced by the lens is at the "image plane." These planes are called conjugate planes and their distance from the lens is described by the following equation:

$$\frac{1}{f} = \frac{1}{o} + \frac{1}{i}$$

where f is the focal length of the lens, o is the distance from the lens to the object being imaged, and i is the distance from the lens to the image plane [47]. The lens makes the planes at distances o and i "conjugate" to one another. Within these conjugate planes, a positional shift in one plane is seen as a positional change in the other. If an object moves within the object plane, or sample plane in the case of these experiments, then the image of that object moves within the image plane. However, translational changes in the object plane turn into angular changes in the light's trajectory in the back focal plane and do not produce any positional changes. Conversely, angular changes of beam path in

the object plane are converted into translational changes in the back focal plane. The back focal plane is, as its name would suggest, one focal distance away from the lens on the opposite side of the object, or sample, plane. Figure 1.5 shows the difference between the sample plane, back focal plane, and image plane for the same lens. In optical trapping experiments translational motions of the bead result in angular deflections of the trapping beam. So, in order to measure a bead's movement with extreme accuracy we take an image of the laser beam at the back focal plane where those angular laser deflections are translated into positional changes.

Trapping laser movement in the back focal plane is detected is by using a lens and a quadrant photodiode (QPD). Photodiodes are detectors that are capable of measuring low levels of light. Photons striking the detector create a cascade of electrons that are amplified and create a measurable signal in either current or voltage [47]. A QPD is merely a photodiode segmented into four sections, or quadrants: Northeast, Northwest, Southeast and Southwest. For the measurements performed here, the difference in voltage between the up and down, (NE + NW) – (SE + SW), and between left and right, (NW + SW) – (NE + SE), is measured. As the Gaussian beam hits the center of the detector, shedding equal light on all four quadrands, both the difference horizontally and vertically will be zero. The QPD is positioned so that these voltages are zero when the bead is at rest in the beam's focus. The lens and QPD are positioned downstream of the sample and condenser lens, such that the lens makes the back focal plane and the plane at the QPD detector conjugate. If the bead moves away from the focus in the sample plane, the beam moves away from the center of the QPD causing a change in the horizontal and/or vertical difference voltage. After proper calibration, this voltage difference can be

translated into accurate position detection of the bead. Example: if the bead moves to the right in the sample plane the beam deflects in an angle to the right. In the back focal plane the beam shifts its position to the right. The back focal plane is imaged onto the QPD, and the beam hits the detector more on the right side causing horizontal difference voltage between the right and left halves of the detector to increase. These differences are normalized by the sum of all four quadrants to keep the position measurement free of any misinformation due to beam power fluctuations. This is how the bead's position is measured. From that, we can determine the amount of force the trap is exerting on the bead.

1.5 The Experiment

It is the goal of these experiments to characterize force-related properties of multiply engaged Eg5, and kinesin-1 motors. Over the years, single kinesin-1 molecules have been extensively studied with the use of optical trap microscopy [26-29]. The amount of force required to dissociate a single Eg5 from the microtubule has also been characterized [44, 48]. However, it is important to step further and understand how multiple motors operate together since this is integral to their functionality *in vivo*. This has recently been performed for up to two kinesin-1 motors transporting cargo *in vitro* by Vershinin et al. [25], and even in *Drosophila* embryos by Shubeita et al. [24]. These experiments were performed on full length kinesin-1 molecules and engaged motor number was determined by way of stall force histogram analysis. Here we study truncated forms of the motors bound to polystyrene beads engaged in transport of the bead along surface-bound tubulin tacks. Through a new and unique form of analysis

involving the observation of stepwise release events, we directly identify up to four motors simultaneously engaged in transport of a bead and examine the properties of these multiple motor transport systems for both kinesin-1 and Eg5. Our goal is to study three separate characteristics pertinent to a molecular motor under strain. First, we will focus on understanding the maximal force that a number of cooperative motors can withstand. We aim to not only characterize single kinesin-1 and Eg5 molecules, but also to model how multiple motors act in conjunction with one another. Second, by studying multiple motors working together we are able to derive the structural rigidity of the molecules in the form of an effective spring constant, and compare the stiffness of the Eg5 motor domain to that of kinesin-1 to determine if the sequence and structure differences between the two alter the protein's rigidity. Finally, by increasing the rearward strain to the point of motor disassociation from the microtubule and then allowing it to rebind, we measure the binding rate of the motor-microtubule interaction. By doing so for a number of motor concentrations, we examine how quickly motors can reattach themselves when disassociation occurs and the concentration dependence of this interaction.

The motor proteins used here are truncated, 560 amino acids constructs of Eg5 and kinesin-1. The construct for kinesin-1, K560, has been widely used in previous experiments providing us with sufficient background concerning the construct's integrity. It exhibits processivity along microtubules similar to native kinesin-1 and is a good construct for studying kinesin-1 properties [12, 23, 49-52]. The Rosenfeld lab (Columbia University, New York) constructed and purified a processive chimera protein to be used as a substitute for native Eg5. It contains the head of Eg5 and the remaining tail of the

K560 construct (Fig. 1.6). This enables our measurements to make a direct comparison between the head regions of Eg5 and kinesin-1.

We use an optical trap to measure release forces for single and multiple Eg5 motor domains and compare them to those of the well studied motor protein kinesin-1. The molecular motors are attached to a polystyrene bead which is manipulated by the trap and brought to nearby axonemes, which are microtubule bundles. The axonemes are affixed to the surface of the sample chamber and remain fixed in the lab frame. Motors attached to the bead bind to the axoneme and, in the presence of ATP, begin walking preferentially towards the plus end. This mobility transports the bead out from the trap's center as the motors walk. Figure 1.7 shows a cartoon depiction of the experiment. The trap supplies a restorative force on the bead attempting to return it to the laser's focal point. For length scales pertinent to the experiment, the magnitude of this force is directly proportional to the magnitude of the bead's displacement from the trap's center. The motors continue to walk and transport the bead, but the restoring force of the trap increases as the bead moves farther from the center until, at the "release force," the motors dissociate from the axoneme and the bead relaxes back to the trap focus. After some time, motors will re-associate with the axoneme and begin the transport process over again. We witness this process happen numerous times for numerous beads at varying motor concentrations. Collecting these events and using a new method of data analysis, we are able to derive all three characteristics we wish to measure; release force for multiple motors, stiffness constant characterizing the motor, and the binding rate.

It should be noted that measuring the release force is different from measuring a motor's stall force, another force characteristic commonly studied for Kinesins. A stall

force is the rearward force required to slow and eventually stop a motor from continuing forward in advancing the bead, or the point at which it stalls. The release force is the force at which the motor becomes completely detached from the track. For the motor protein kinesin-1, the release force and stall force are very similar in magnitude and near stalling can either be directly witnessed before detachment or extrapolated from velocity vs. force curves [29, 53, 54]. In the case of Eg5, the detachment from microtubules occurs far before the stall event so it cannot be directly observed. Previous predictions by Valentine et al. [44] place the stall force for individual Eg5 motors at ~9 pN by projecting the force-velocity curve to the point at which the motor speed is zero. This value is much higher than release forces measured here, ~4.7 pN.

1.6 Figures

Figure 1.1

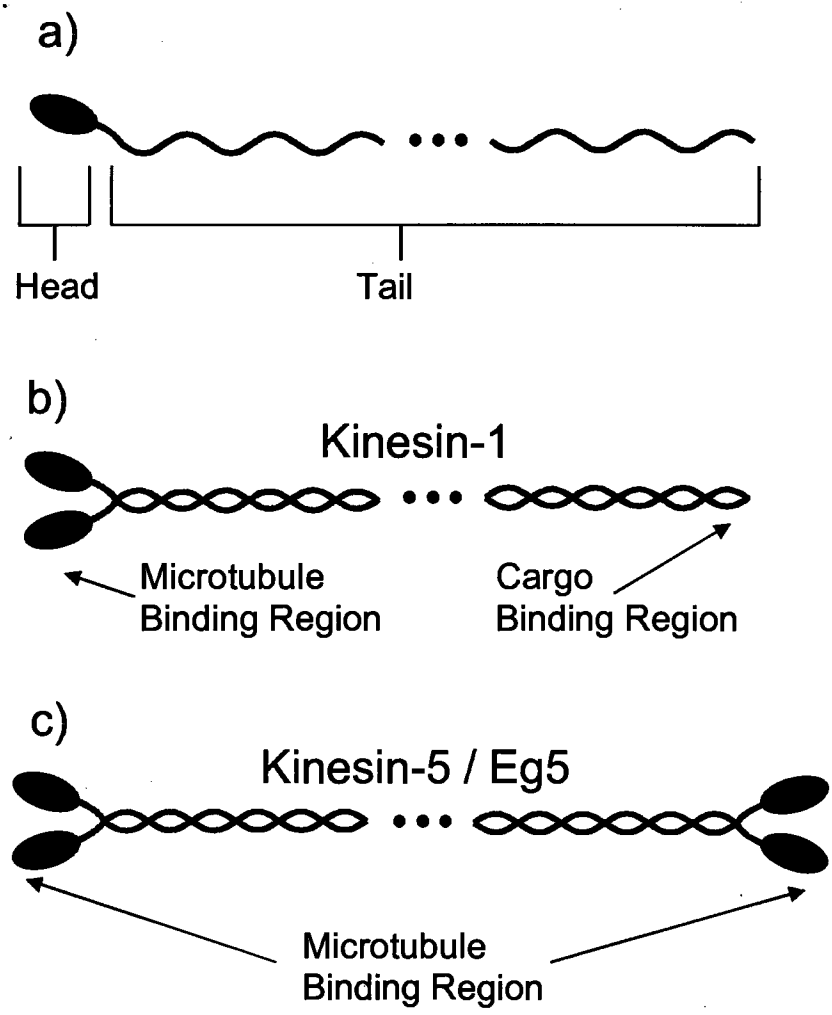

Figure 1.1: Cartoon depictions of molecular motors. a) The structure for a Kinesin protein molecule. The N-teminal head is a globular region that houses the ATP hydolysis domain and a binding site for microtubules. The tail is an α-helical region that extends ~700aa beyond the head. b) Dimeric structure for a Kinesin-1 motor. Cargo transported by kinesin-1 binds to the C-terminal end while motility along microtubules occurs at the heads. c) Tetrameric structure of Kinesin-5 motor. The C-terminal ends of the four molecules combine creating a protein structure with two, two-headed ends, each capable of binding and translating along microtubules.

Figure 1.2

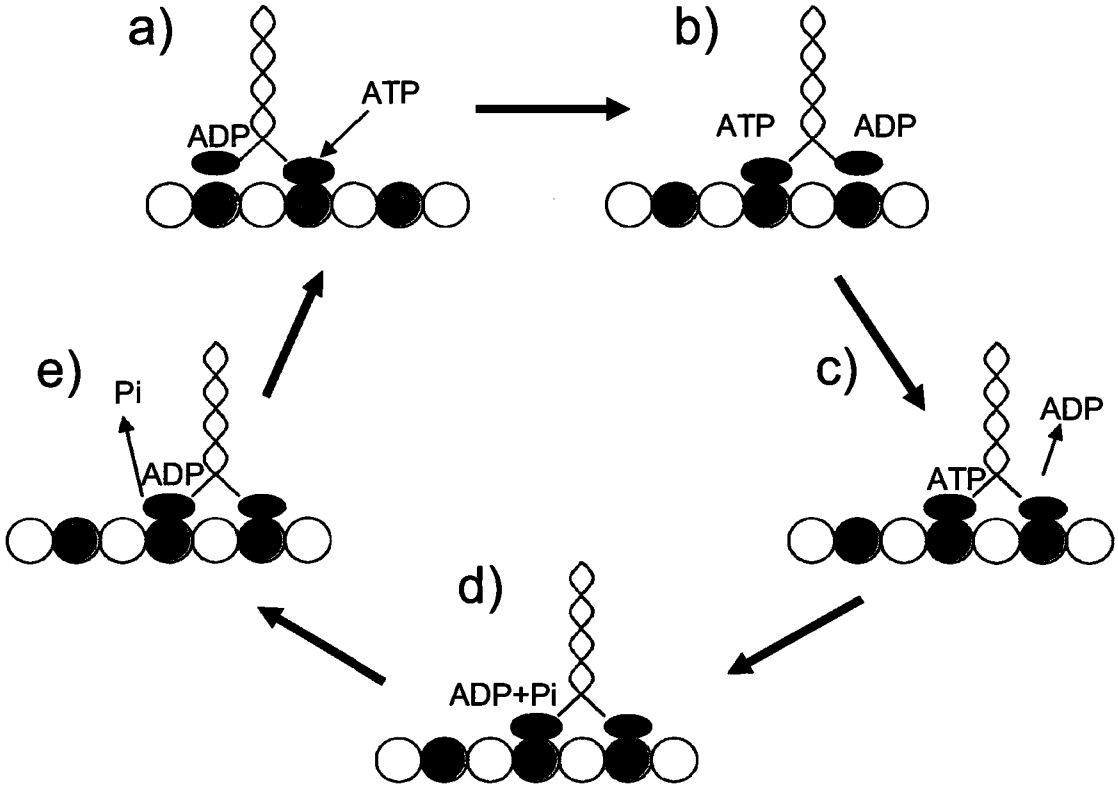

Figure 1.2: The ATP cycle of kinesin-1 stepping. a) The trailing head contains ADP and is unbound from the microtubule while the leading head is about to receive ATP. b) ATP enters the bound head and the protein takes a step forward as the trailing head becomes the leading head. c) ADP is released and the head binds to the microtubule. d) ATP is hydrolyzed. e) The phosphate group is released and the tailing head unbinds from the microtubule.

Figure 1.3

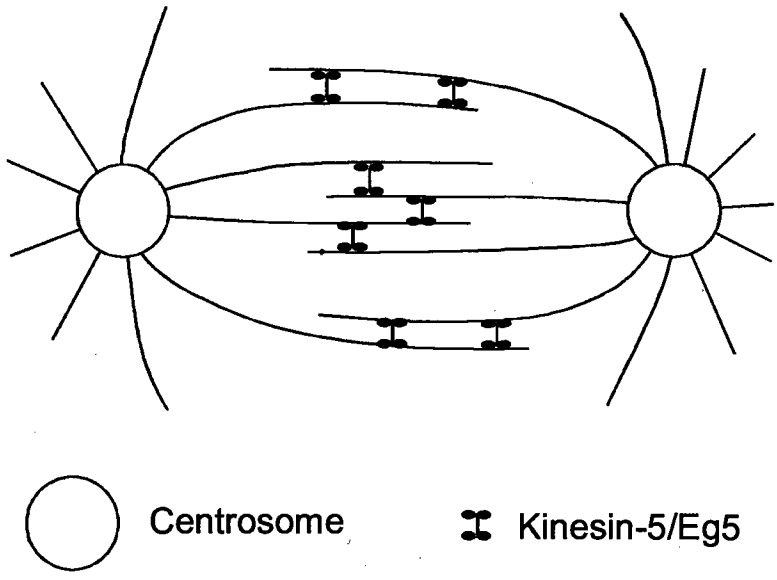

Figure 1.3: A diagram of proper spindle formation from the crosslinking of microtubules by the Kinesin-5 motor Eg5. Microtubules protruding from the two centrosome poles aggregate in the cell center due to the tetrameric Eg5 motors crosslinking them.

Figure 1.4

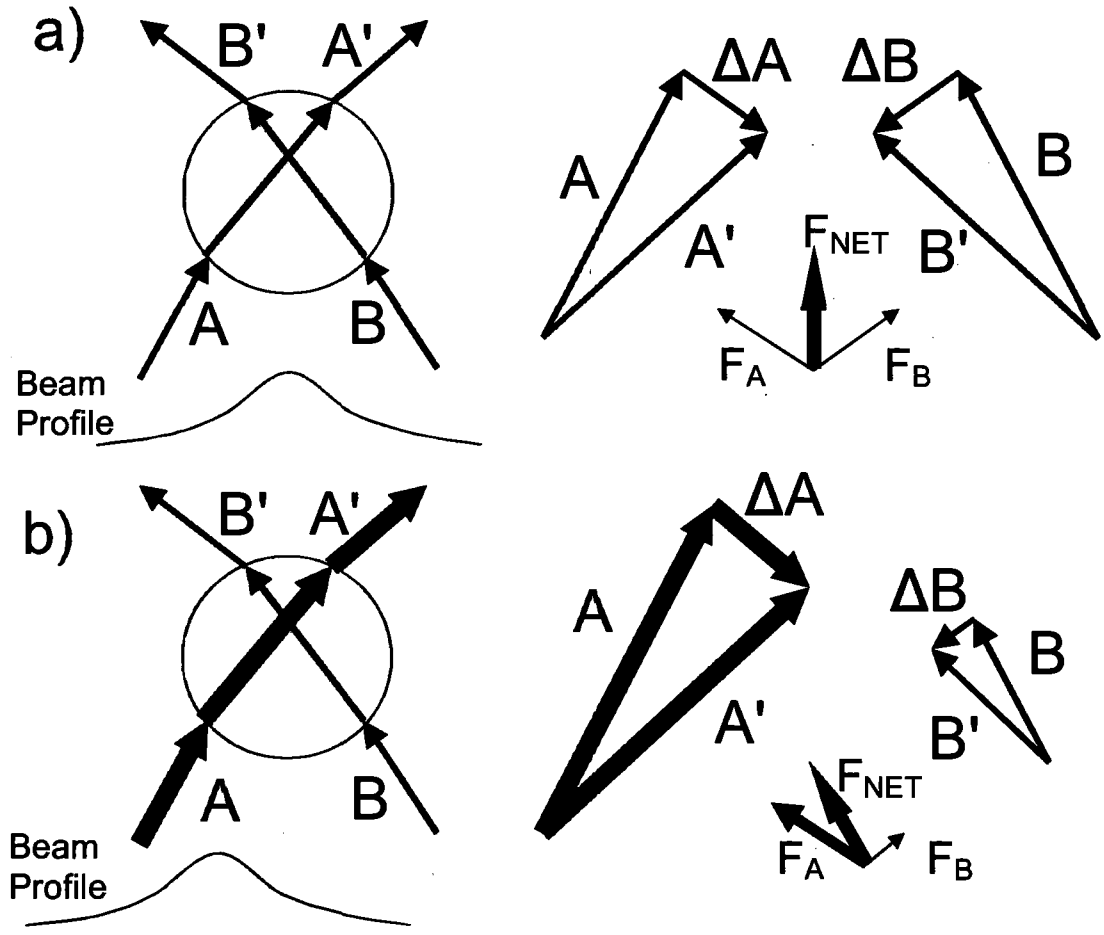

Figure 1.4: Classical ray-diagram depiction of optical trapping. a) The bead center is below the center of the trap. The intensity profile of the trapping laser is shown below the bead. Paths of sample rays A and B are drawn passing through the bead. Their vector differences before and after the bead are shown to the right. The change in direction of the photon ray depicts a change in momentum and corresponding forces felt by the bead are shown below. Forces from ray A and ray B add to give a net force in the upward direction. b) The bead center is above and to the right of the trap center. The vectors A and B have the same direction as in the previous example, but, because of the beam profile, ray A is of a higher magnitude that ray B. This results in a force that is not only upward, but also to the left as the leftward pull of ray A is stronger than the rightward pull of B.

Figure 1.5

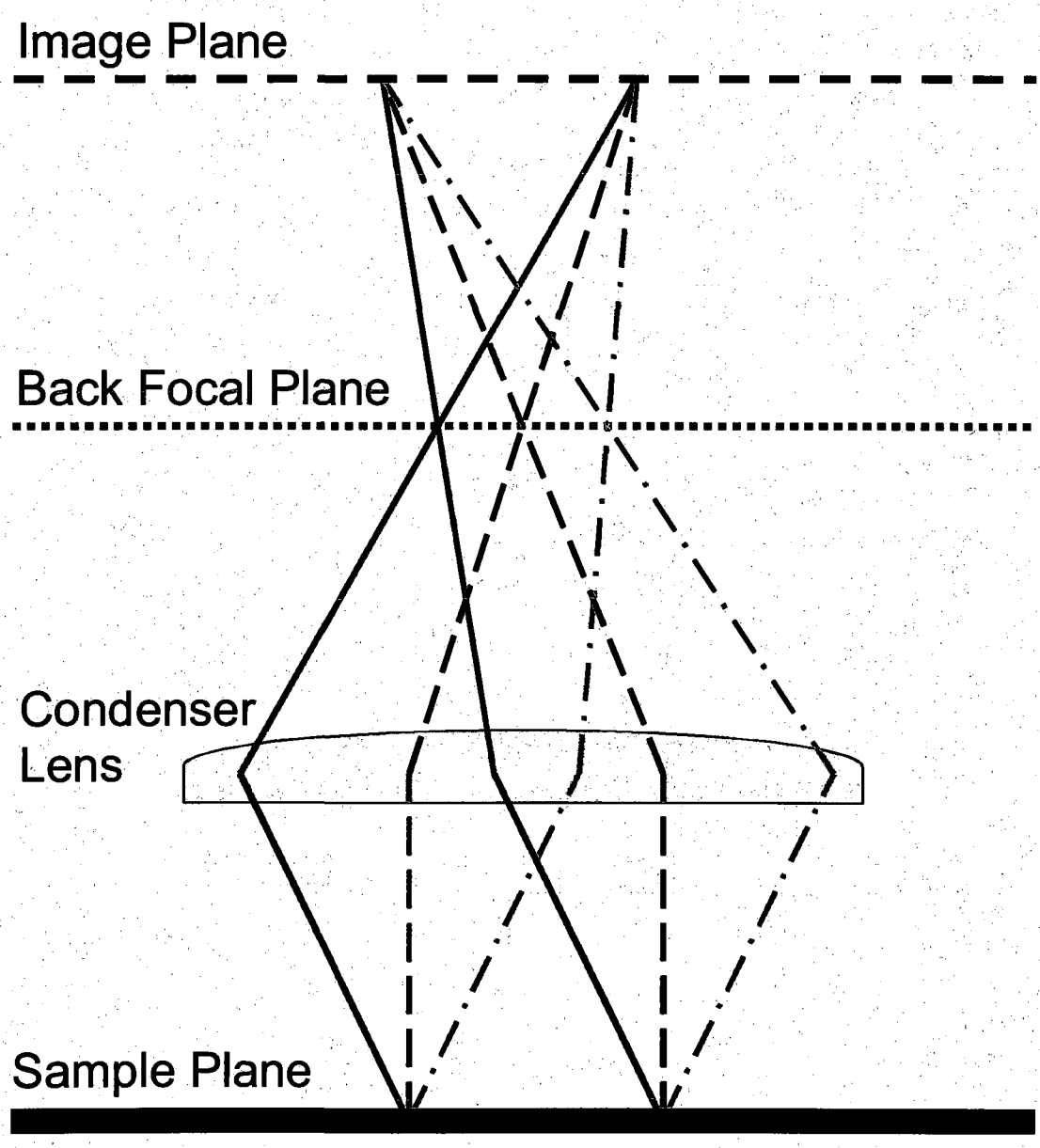

Figure 1.5: Different optical planes defined by a plano-convex lens. Three pairs of rays of light originating from the sample plane are traced out for the sake of illustration, solid rays, dashed rays, and dotted-dashed rays. Each pair has a distinct incident angle at the sample plane. Both rays in the pair share the same angle, but come from different locations. Rays originating from the same position in the sample plane end in the same position in the image plane, regardless of incident angle in the sample plane. Therefore, the sample plane and the image plane are conjugate. However, rays with the same incident angle at the sample plane end in the same position in the back focal plane, regardless of their point of origin.

Figure 1.6

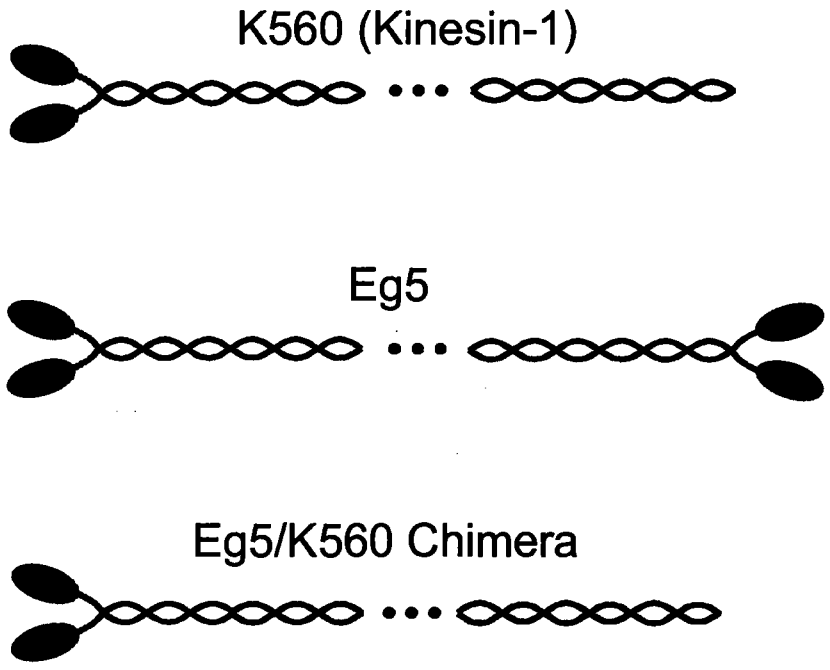

Figure 1.6: Construction of the Eg5/K560 construct used in these experiments. K560 is the truncated version of human kinesin-1. The Eg5/K560 chimera has the head and partial tail regions of human Eg5 but is spliced with a majority of the coiled-coil region of K560. These two constructs, K560 and the Eg5 chimera, are the two molecular motor proteins that will be studied and compared here. The nature of these constructs allows us to deduce that any difference in characteristic properties between the two must stem from differences in the head and forward tail region.

Figure 1.7

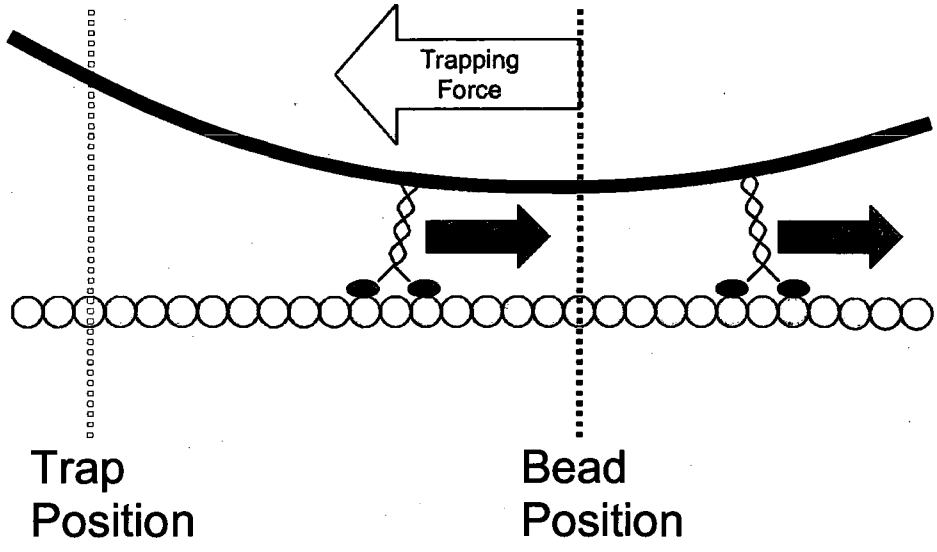

Figure 1.7: Optical trapping experiment. The optical trap is in a fixed position as the motor proteins process along the tubulin track transporting the large bead to the right. As the position of the bead's center of mass moves to the right, the trap applies a force on the bead in the direction of the trap's position, to the left.

CHAPTER 2: MATERIALS AND METHODS

The experiment required biological samples to be prepared, the optical trapping apparatus to be constructed, and the form of data analysis to be devised. This chapter describes the sample preparation, experimental setup construction and the specifics of data analysis that we implemented to conduct the research.

2.1 Biological Samples

2.1.1 Eg5 and Kinesin-1 Constructs

Kinesin-1 mutants are truncated to 560 amino acids in length, which is a very commonly used version of the full length [55]. (For kinesin-1 and Eg5 the full length is ~1000 aa [36]) The Eg5 motor is reduced from its native homotetramer to a dimer. It is suspected that, *in vivo,* only one dimeric end walks along a microtubule at a time during the cross-linking of mitotic spindles [35]. We use a dimeric construct to localize one half of Eg5 without interference of the other. From a region near the head through to the C-terminus, our mutant Eg5 was replaced with that of kinesin 560 (Fig. 1.1). With this, we narrow our force studies to the properties of the motor's microtubule binding domain through to the truncation point. By comparing K560 to this Eg5 chimera we localize our study and characterization to the region pertinent to binding and force generation of the motor. Differences in measurements between the two motors rise from dissimilarities within this area as all other aspects of the experiment are constructed to be identical.

2.1.2 Purification of K560 and Eg5

Kinesin-1 mutant K560 was purified by Benjamin Blehm and Erdal Toprak in our lab according to the protocol outlined by Pierce and Vale [56]. The DNA that sequenced the protein was a gift from the Vale lab (University of California, San Francisco). The K560 mutant contained a green fluorescent protein insert and a 6X histidine tag at the C-terminus.

The Eg5 chimera was created and purified in the Rosenfeld lab (Columbia University, New York) then shipped to our lab for long term storage and use.

2.1.3 Sample Preperation

The following protocol is a modified version of those outlined previously by Yardimci et al. [51].

In a 500 μL Eppendorf centrifuge tube, 5 μL of a stock of 1% w/v 1.2 μm diameter, streptavidin coated polystyrene particles (SVP-10-5, Spherotech Inc., Lake Forest, IL) were added to 43 μL of PEM80 buffer (80 mM Pipes at pH 6.9, 2 mM $MgCl_2$, and 1 mM EGTA) and sonicated for 2 min at ~4°C to break up any bead aggregates that formed during storage. 2 μL of a 1 mg/mL stock of biotinylated anti-histidine antibody (MCA1396B, AbD Serotech, Raleigh, NC) were then added and the sample was allowed to react for 30 min at 4°C under gentle agitation, ~240 rpm. During this phase, the biotin binds to the streptavidin covalently bonded to the polystyrene spheres. The biotin-streptavidin protein bond is very strong, with a dissociation constant of approximately 4 x 10^{-14} M^{-1} [57], producing a tight coupling between the bead and the anti-histidine

antibody. After this reaction period, 50 μL of 8 mg/mL bovine serum albumin (BSA), dissolved in PEM80, was added to mitigate protein and bead adhesion to the centrifuge tube inner wall. The sample was allowed to sit at this stage for 10min on ice and then centrifuged at 15,000 x *g* for 15 min at 4°C to rid the sample of excess biotinylated antibodies. The supernatant was aspirated off and discarded, and the pellet was suspended in 8 mg/mL BSA. After another round of centrifugation at 15,000 x *g* for 15 min at 4°C the supernatant was again discarded to rid any more excess antibodies and the pellet was re-suspended in 9 μL of PEM80+ buffer which consists of 8 mg/mL BSA, 10 μM ATP, and 2 mM dithiolthreitol (DTT) in PEM80 buffer. (The DTT is added to separate any protein aggregation occurring from the formation of disulfide bonds. Such aggregation has the potential to inhibit mobility of the molecular motors. The ATP is added to stabilize the motor protein. Our lab has discovered that kinesin-1 motors destabilize and do not retain mobility if no ATP or ADP is added to the solution.) The beads were then sonicated for 2 min at ~4°C to disperse any particle aggregates that occurred during the centrifugation process. A stock aliquot of motor protein, 6 μM in concentration for kinesin-1 and 18 μM for Eg5, was removed from the -80°C storage freezer and thawed on ice. The motor protein was diluted to 200 nM, 60 nM, or 2 nM, depending on the experiment, in PEM80+ buffer. Then 1 μL of the dilution was added to the bead solution to allow the anti-histidine antibodies attached to the beads to bind to the 6X-histidine motif that had been engineered onto the C-terminus of the motor protein. This step was allowed to occur on ice for 3 hrs. At this point, the concentration of beads was ~10 pM and the motor concentration was 20.0 nM, 6.0 nM, or 0.2 nM, depending on the experiment, producing a bead to motor ratio of 1:2,000, 1:600, or 1:20. Figure 2.1 is

a cartoon depiction of how the motor proteins are attached to the bead in these experiments.

Near the end of the reaction, a sample chamber was constructed (described later) and axonemes (purified from sea urchin according to the protocol described by Pierce and Vale [56]) were diluted 20-fold in PEM80 and ~15 μL of this solution were flown into the chamber. Axonemes were allowed to adhere to the inner surface of the cover glass for 5 min while resting on ice. The chamber was then flushed with 100 μL of PEM80 with 8 mg/mL BSA for 5 min to remove unbound axonemes and to coat the glass surface with BSA mitigating future non-specific binding of the beads. The bead-motor sample was sonicated at ~4°C for 1 min, to break up aggregates that may have occurred during the 3 hr reaction time, and then diluted 100 fold in the following buffer: PEM80, 2 mM ATP, 2 mM DTT, 2.5 mM protocatechuic acid (PCA), and 50 nM protocatechuate-3,4-dioxygenase (PCD). (PCA and PCD combine to create an oxygen scavenging system. Together they remove harmful free oxygen radicals present in the solution [58].) 20 μL of the sample solution was flown into the sample chamber which was then taken to the optical trap microscope setup for experimentation.

2.1.4 Sample Chamber Construction

This protocol is similar to the one outlined for optical trap experimentation by Appleyard et al. [59].

Number 1.5 cover glasses, 30 x 22 mm and 0.16 – 0.19 mm thick, were rinsed once with isopropyl alcohol to dissolve organic contaminants, and then once with doubly deionized water before being placed in a plasma cleaner (PDC-001, Harrick Plasma,

Ithaca, NY). Argon gas was used in the plasma cleaner and after pumping the pressure down to vacuum (~200 mTorr) the radio frequency (RF) oscillating field were activated on the low setting (716 V DC, 10 mA DC, 7.16 W applied to the RF coil). (It should be noted that argon was used for ablative cleaning because of its inert properties. It was recommended by the plasma cleaner manufacturer, Harrick Plasma, that using room air or any other gas mixture that contained oxygen ran the risk of oxidizing the glass surface. This oxidized surface might have properties hazardous to biological samples. No control experiments were designed or implemented by the author to confirm or refute this claim.) Cover glasses remained under the argon plasma for 5min while contaminates were removed by plasma ablation. After cleaning, they were removed and stored in a plastic container, shielding them from dust and airborne contaminants, at room temperature until use. Although both sides of the glass were cleaned with isopropyl alcohol, only one side of the cover glasses was ablated due to the construction and nature of the plasma cleaner. This plasma cleaned side was used on the interior of the sample chamber, the portion in contact with the sample, once constructed.

Sample chambers were constructed by placing two ~4 inch pieces of double-sided sticky tape long ways over a 3 x 1 inch glass slide leaving ~1/4 inch space in between that ran the length of the slide along the center. Next, a plasma cleaned cover glass was centered and placed on the slide, keeping the ablated side down and facing the slide, adhering to the tape. Extra pressure was applied to the glass using a clean pipette tip to ensure adhesion. The excess tape was cut away at the edges of the cover glass using a razor blade and discarded. The chamber was then ready for experimentation.

2.2 Optical Trap

An optical trap, similar to that described by Yardimci et al. [51], was used to make force measurements of the motor proteins. A bead, decorated with molecular motors as described earlier, was caught in the trap and positioned near an axoneme adhered to the sample chamber surface. The active motors bound to the axoneme and began transport of the bead away from the center of the trap. The rearward force implied on the bead by the trap was proportional to the displacement of the bead according to the equation described earlier $\mathbf{F}_{trap} = -\kappa \mathbf{d}_t$, where κ is the stiffness constant of the trap and $\mathbf{d}_t$ is the distance between the center of the trap and the center of the bead. The following is a description of the trap's construction and how it was calibrated for our force experiments.

2.2.1 Optical Trap Setup

Figure 2.2 is a diagram of the optical trap setup used for the work described here. The actual position where the bead is trapped is within the Nikon microscope (TE2000-U, Nikon Inc., Melville, NY) between the microscope objective (Apo VC 60x/1.20 WI inf/.15-.18 WD .27, Nikon Plan) and the condenser lens (WI .9 Nikon). The sample chamber rests on a piezoelectric stage capable of X, Y and Z translation (MCL 01069, MCL 01166, NanoDrive MCL 01312, Mad City Labs Inc., Madison, WI). The objective focuses the beam down to a point where the trapping happens and the condenser lens after the sample chamber then creates a back focal plane that is imaged onto the QPD detector (QP154-Q-T01032 mounted on QP-SD2 PCB, Pacific Silicon Sensor Inc., Westlake Village, CA) by way of lens 5 (1145-C, Thorlabs Inc., Newton, NJ) with a focal

length of 75 mm. Before light enters the detector other wavelengths aside from 1064nm are removed with an emission filter (Z1064/10x, Chroma Technology Corp., Rockingham, VT). A neutral density filter (NE220B, Thorlabs) also attenuates the beam by one hundred fold to protect the detector from over exposure. Data is collected from the QPD into a computer through two data acquisition cards (PCI-6052E, PCI-6733, National Instruments, Austin, TX) and gathered with home coded software in LabView. This is the heart of the experimental setup where trapping occurs and how the measurement is taken.

The rest of the setup is designed for ease of alignment and detection. The laser itself is a 1064 nm diode-pumped Nd:YAG (BL-106C, Newport Corp., Mountain View, CA) with a J series power supply (J2OI-8S-12K-NSI, Newport). IR wavelengths are selected in optical trapping experiments due to the fact that aqueous solutions and biological samples are almost completely transparent to photons at that energy. The linearly polarized beam passes through a half-wave plate (WPH05M-1064, Thorlabs) and into a polarizing beamsplitter cube (05FC16PB.7, Newport) that acts as a laser attenuator. By adjusting the wave plate one can allow more or less laser power to be sent into the experiment while the rest is diverted into a beam block (LB1, Thorlabs). A couple of lenses are then used to expand the beam by approximately six times. Figure 2.2 depicts them as lenses 1 and 2, but due to the nature of space on the actual setup this is broken down into two Keplerian telescopes of two lenses a piece, four lenses total, of focal lengths 35mm, 100 mm, 100 mm, and 200 mm (LA1027-C, LA1509-C x2, LA1708-C, Thorlabs). Two more lenses form another Keplerian telescope before the microscope that serves two purposes. One is to expand the beam enough to fill the back aperture of the

microscope objective to create a good strong trap. The larger the incoming beam the more tightly it is focused down at the sample plane, creating a greater photon gradient, creating a stronger trap. The second purpose of this telescope is for beam alignment, to make sure the beam enters the microscope lens straight and through the center. These lenses are positioned in a specific way to serve more purposes in other experiments, but the work here does not utilize this so it will not be discussed at this time. Lens 3 has a focal length of 60mm and lens 4 has a focal length of 125mm (1401-C, 1384-C, Thorlabs).

In order to visualize the trap and the sample light is sent into the microscope and collected by a CCD camera (DV887DCS-BV, Andor Technology, South Windsor, CT). A halogen lamp (20500/34, Optical Analysis Corp., Nashua, NH) is attached to the Nikon microscope and sends white light through the condenser lens, creating a field of Köhler illumination in the sample. The light is then collected through the objective and reflected within the microscope and imaged onto the CCD camera. To separate the white light from the 1064 nm laser beam two dichroic mirrors were used to pass the white light and reflect the trapping/detection beam. Above the sample chamber the dichroic was a custom built 1" x 3" mirror transmitting 460-750 nm and reflecting 850-1080 nm and composed of a laser grade substrate with anti-reflective coating from Chroma. The other dichroic mirror below the sample chamber reflected everything above 800 nm and passed every wavelength below 800 nm (800 DCSX, Chroma). Before reaching the CCD camera, the illumination light is further cleaned up by an emission filter (HQ535/50 M-2P, Chroma) that removes any reflected 1064 nm light. The camera then images the

sample allowing the user to examine the position of beads, the trap and axonemes adhered to the sample chamber surface.

2.2.2 Calibration

Experimental information comes to the user in the form of normalized difference voltages from the QPD. To translate these normalized difference voltages into force applied on the bead by the trap, there are two values that must be determined first. One is the conversion from normalized volts to position, in nanometers. Second is the conversion from position to force or, simply, the trap stiffness, κ.

2.2.2.1 Position

Determining the conversion factor between normalized QPD difference voltages and nanometer movement of the bead in the sample plane was done according to the protocols outlined in Visscher et al. [60] by scanning an immobilized bead through the stationary trapping beam using a sensitive piezoelectric-motor driven stage. To do so, a sample chamber was created containing 1.2 μm, streptavidin-coated microspheres attached to the surface by means of non-specific binding. These are the same type of beads used for the motor experiments. Free floating beads in 8 mg/mL BSA were flown into the chamber 30 min later. The BSA coats the sample chamber surface preventing further adhesion of the beads and allowing a number of the spheres to remain free-floating within the sample. The chamber was sealed with epoxy at both ends and taken to the optical trap setup. (This sealing process prevents evaporation and confines the liquid providing complete coupling between sample chamber movements and liquid sample

movements.) A free floating bead was captured by the trapping laser and the piezoelectric stage, holding the sample chamber, was raised until the bead made contact with the surface. This ensured that the trap center was at the proper height when next examining beads stuck to the surface. The free bead was loosed, the trap was positioned next to a bead already immobilized on the surface and the stage was programmed to scan the bead through the trap in a two-dimensional 1.8 x 1.8 μm grid in intervals of 50 nm. The approximate center of the bead was determined by finding and fitting a line between the highest and lowest points of the difference voltages in the x- and y-directions. Where they intersected was the centroid of the bead. The piezoelectric stage was moved so that the center of the bead was at the trap focus. The stage then scanned the bead vertically, returned to center, and then horizontally through that center in intervals of 20 nm creating QPD voltage difference vs. position curves for the x and y axes. The regions near the center of the bead were linearly fit, the inverse of the slope being the conversion factor from normalized QPD voltage to bead position in nanometers we call β. This is the calibration factor we were looking to acquire. Our setup is characterized by a β_x value of 918 nanometers per normalized volt in the x-direction and 1059 nanometers per normalized volt for β_y in the y-direction.

2.2.2.2 Stiffness

The conversion factor between normalized QPD voltage and force applied by the trap was determined using the power spectrum fitting technique outlined by Svoboda and Block [61]. The theory takes on the following form. A bead caught in the trap has three

sources of force acting upon it; the trap, viscous drag, and thermal fluctuations. Writing down our equation of motion we have:

$$F_{THERM} = \gamma\dot{x}(t) + \kappa x(t)$$

γ is the viscous drag and F_{THERM} is the thermal noise which follows:

$$F_{THERM} = \gamma\sqrt{2D}\xi(t)$$

D is the diffusion coefficient $D = k_B T/\gamma$. k_B being the Boltzman constant, T is room temperature, and $\xi(t)$ represents the normalized white noise fluctuations defined by $\langle\xi(t)\rangle = 0$ and $\langle\xi(t)\xi(t')\rangle = \delta(t-t')$. Taking the Fourier transform of the force equation we arrive at.

$$\gamma\sqrt{2D} = \gamma(2\pi i f)\hat{x}(f) + \kappa\hat{x}(f)$$

Now, create the power spectrum, $P(f)$, by solving for the Fourier transform of position, $x(f)$, and taking its magnitude squared we have:

$$P(f) = \frac{D}{\pi^2\left(f^2 + f_c^2\right)}$$

Here $f_c = \kappa/(2\pi\gamma)$. Now, we can capture a bead in our setup, measure its position $x(t)$ over time, evaluate the power spectrum numerically from the data, and fit that power spectrum with the equation above, a Lorentzian function, to determine D and f_c. Knowing those we can easily arrive at the trap stiffness because, from our previous definitions for D and f_c, we get:

$$\kappa = 2\pi f_c \frac{k_B T}{D}$$

Taking the theory and putting it to practice, we captured a free floating in the trap and its QPD position was measured for 20s at a sampling rate of 16,384Hz. (The fast

Fourier analysis required to compose the power spectrum required the data to be sampled with a frequency equal to a power of two.) The difference voltage data were converted to positional data using the β values calculated earlier. Power spectrums for both the x and y axes of motion were created and fit to the Lorentzian curve, described prior, to get the values of D and f_c. These two parameters having been determined, the trap stiffness, κ, was calculated from the equation above. This procedure gives the trap stiffness in both the x and y directions so one can relate bead distances from the center, $\mathbf{d}_t$, to forces exerted by the trap as $\mathbf{F}_t = -\kappa\mathbf{d}_t$. All calculations, power spectrum analysis and fittings were preformed with MATLAB (Mathworks Inc., Natick, MA) software written in house (Appendix A.1, A.2).

Performing this calibration technique produced stiffness values of 0.0394 pN/nm in the x-axis and 0.0461 pN/nm in the y-axis for an incoming laser power of 36 mW. (The laser power was measured before the beam entered the Nikon microscope apparatus. This is prior to the beam reflecting off of a dichroic mirror and passing through the objective. A few percent of the power is suspected to be lost within these optics, but the effect is negligible.) These stiffness values were used for experiments where the bead to motor mixing ratios were 1:20 and 1:600. For the largest concentration of protein, 1:2,000 bead to motor mixing ratio, it was observed that the motors were capable of carrying the bead a significantly greater distance before reaching the release force. This caused transportation of the bead out of the linear regime of β, the conversion between normalized QPD voltage and bead position. This region is dependent on the bead size and extends ~25% of the bead's diameter, ~300 nm, from the center of the trap. In order to keep the beads from escaping this linear area of position conversion the trap stiffness

needed to be increased. The laser power was raised to 158 mW producing stiffness values of 0.1567 pN/nm in the x-axis and 0.1890 pN/nm in the y-axis. The larger stiffness ensured that the motors transporting the bead would reach their release force before escaping the 300 nm threshold.

2.3 Experiment

Motor coated beads were caught in the trap and brought to close proximity of axonemes allowing the Eg5 or kinesin-1 to bind and, in the presence of ATP, transport the bead towards the plus end. This mobility transported the bead out from the trap's center as the motors walk. The trap supplied a restorative force on the bead attempting to return it to the laser's focal point. This increased as the bead moved farther from the center until, at the "release force," the motors dissociated from the axoneme and the bead relaxed back to the trap focus. We call this a "release event." After some time, motors re-associated with the axoneme and began the transport process over again. We witnessed this occur numerous times for numerous beads at the three motor concentrations. Motions of the particle were captured by the QPD sampled at a rate of 1 kHz for 100 s per data acquisition run. Only three runs, at most, were performed on a single bead before it was released from the trap and a new bead was acquired to ensure a diverse sampling of the population. Several hundred release events were captured for each of the two motors and each of the three mixing ratios of bead to motors. Using our new method of data analysis, described later, we were able to accurately determine the number of motors that are engaged at the time of each individual release event. From this,

we were able to derive all three characteristics we wished to measure; release force for multiple motors, stiffness constant characterizing the motor, and the binding rate.

2.4 Data Analysis

Traces of the bead's position from the center of the trap in both the x and y dimensions were analyzed using MATLAB programs written in house (Appendix A.3). All position points from a data run were plotted and fit to a line. This represented the axis of the axoneme and the direction of the motor's travel. All of the two-dimensional points were then projected onto that line and plotted as one-dimensional travel along that line. This was the trace of the bead along the axoneme. A baseline, the value of position in this one-dimensional projection where the bead is at rest in the focus of the trap, was outlined by the user by selecting a region believed to be free of motor engagement. The points within this selection were averaged to determine the baseline level and their standard deviation was determined to characterize the error in that particular experimental run. The trace rose from the baseline as motors moved the bead away from the trap center, and then fell sharply back to the baseline as the motors dissociated from the axoneme. These release events were noted and the release force, the force exerted on the bead at the moment of motor detachment, was recorded. The release force value was taken by averaging the 50 points representing 50 ms prior to the release event. In order to be considered a proper release event, the trace also needed to withstand the following criteria. The rise in position from the baseline must have occurred over at least 50 ms and reached a distance greater than two standard deviations above the baseline. Each

release trajectory from peak to baseline cannot have exceeded 20 ms and must have ended with the bead's position within one standard deviation of the baseline.

Data analysis that has never before been reported, to the knowledge of the author, was performed here that allows the direct determination of the number of motors engaged with the tubulin track while observing the bead position vs. time trace for stepwise release events. When observing the traces for bead releases, a number of dissociation events occurred in a stepwise fashion instead of an immediate and complete return to the trap center. In other words, motors attached on a single bead did not dissociate from the axoneme at the same time, but, under the experimental conditions here, detached sequentially. Further analyses, described later, suggested that this occurred more often than not. The evidence that these stepwise release events occur can be seen in the force traces (Fig. 2.3). During a release event, as the trace traveled back to the baseline, the position of the bead halted at a "step", for a perceptible amount of time, and then continued its descent to the trap center. We will postulate here and affirm later that each step in the bead release event corresponded to a separate motor disassociating from the tubulin track. Motors carried a bead out from the center of the trap and, sequentially, dissociated from the axoneme. These dissociation events were separated in time longer than the temporal resolution of the experiment. So, we were able to capture the release states; the N motors attached state, the N - 1 motors attached state, and so on. We recorded the release force and categorized them by whether they release in one, two, three, or four steps, corresponding to the number of motors engaged before the release occurred. Examples of release events for varying number of steps are shown in figure 2.4. In order to be counted as steps within a single release event the following criteria must

have been met: a) each stepwise drop must not have exceeded 20 ms, b) step plateaus were required to last for at least 5 ms, c) step plateaus must have been at least 10 nm from one another to ensure that an entire motor had released, instead of just a single head of the two-headed motor, and d) during a sequential step, the trace must not rise again above the value of any previous steps.

2.5 Figures

Figure 2.1

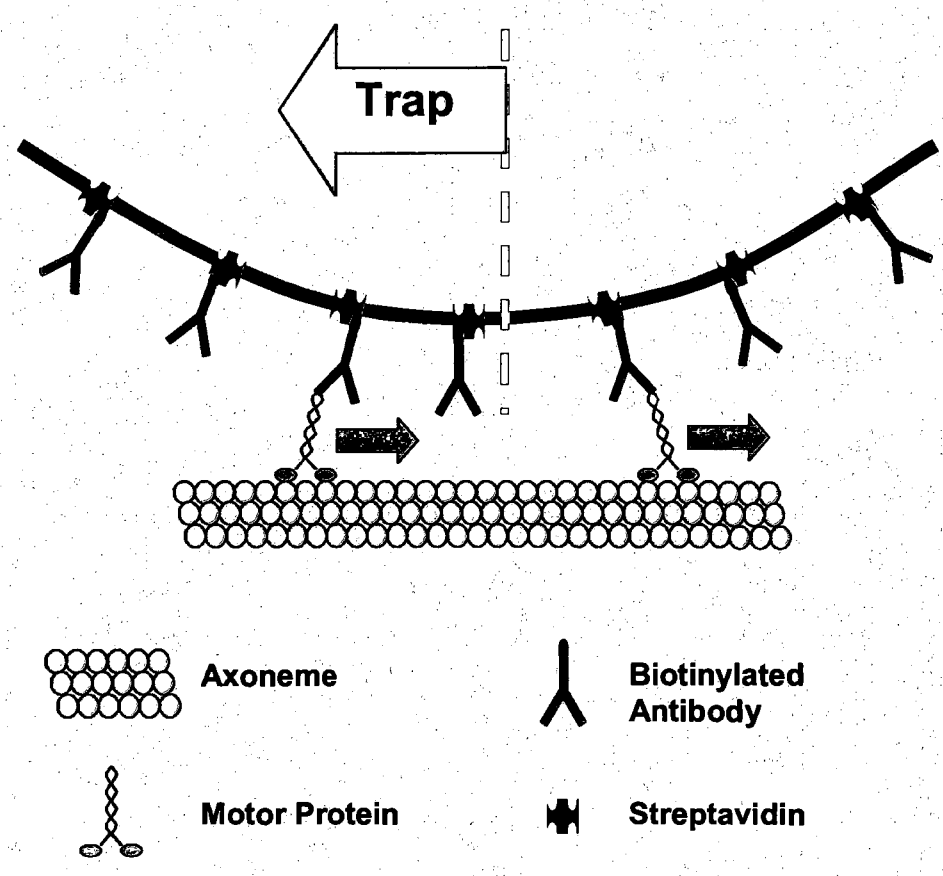

Figure 2.1: A cartoon depiction of the motor-bead attachment and the optical trap experiment. A polystyrene sphere coated with streptavidin binds to biotinylated anti-histidine antibodies. The antibodies bind to the motor protein under study. The motor-coated bead is manipulated with an optical trap apparatus and brought near an axoneme attached to the surface of the sample chamber. Motors engage the axoneme and preferentially transport the bead towards the plus-end of the axoneme. The trap produces a force on the bead opposite to the direction of motion.

Figure 2.2

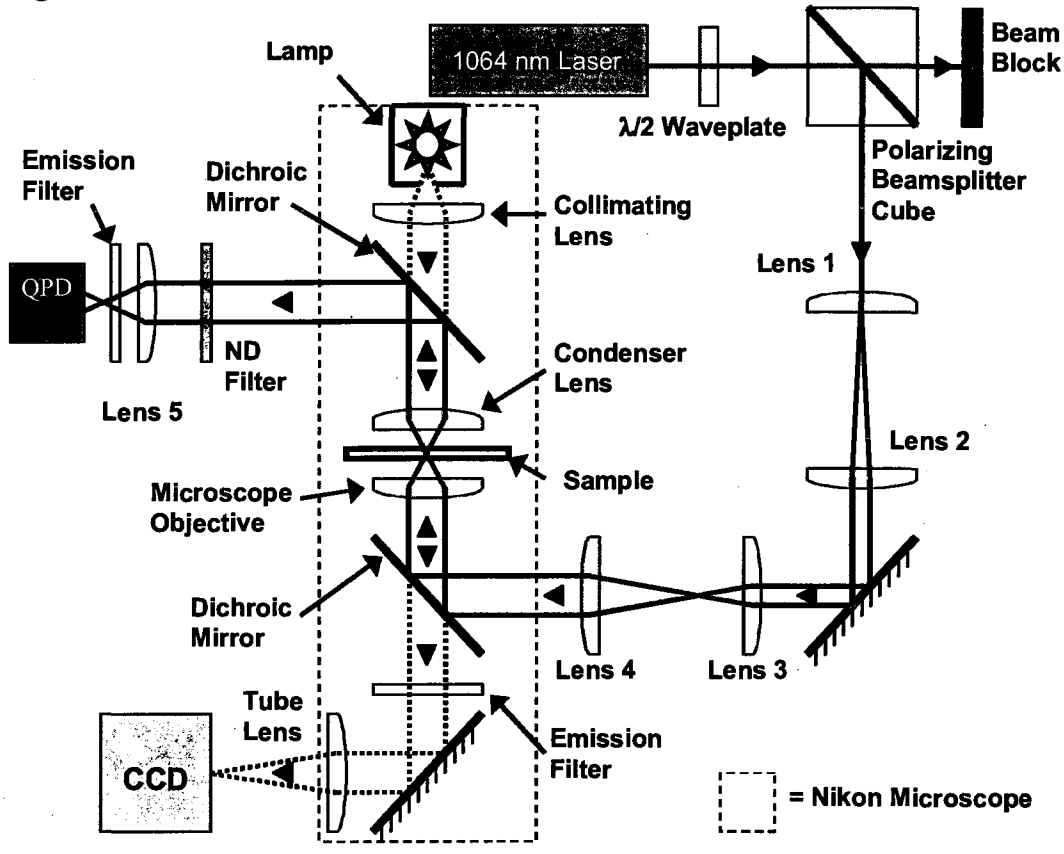

Figure 2.2: Diagram of the optical trap setup. Objects within the dashed line are pieces of the Nikon IX-70 microscope assembly. The path of the 1064 laser beam is the solid red lines beginning at the laser head, traveling upward through the sample and ending at the QPD detector. The path of the white lamp illumination is the dotted black line beginning at the lamp, traveling downward through the sample and ending at the CCD camera.

Figure 2.3

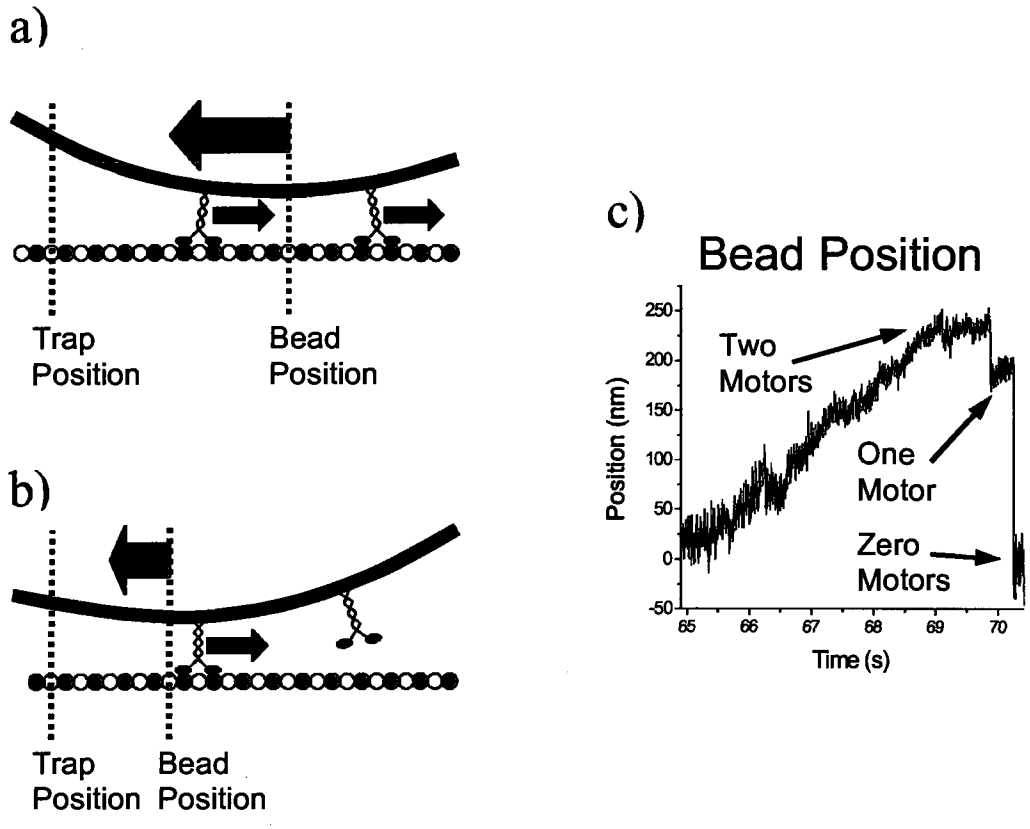

Figure 2.3: Stepwise release event for the two engaged motor scenario. a) Two molecular motors transport the bead away from the trap center. As the beads process further to the right, the trap exerts an increasing rearward force. At some distance during transport, the release event occurs. b) One motor releases leaving only one motor engaged. The release of one motor allows the bead's center of mass to shift closer to the trap center. c) The position trace, a plot of the bead's distance from the center of the trap versus time, shows a rise in the beginning as the two motors transport the bead, a short fall as one bead detaches leaving one motor engaged, and a subsequent fall to the baseline as the second motor dissociates leaving no motors left to transport the bead.

Figure 2.4

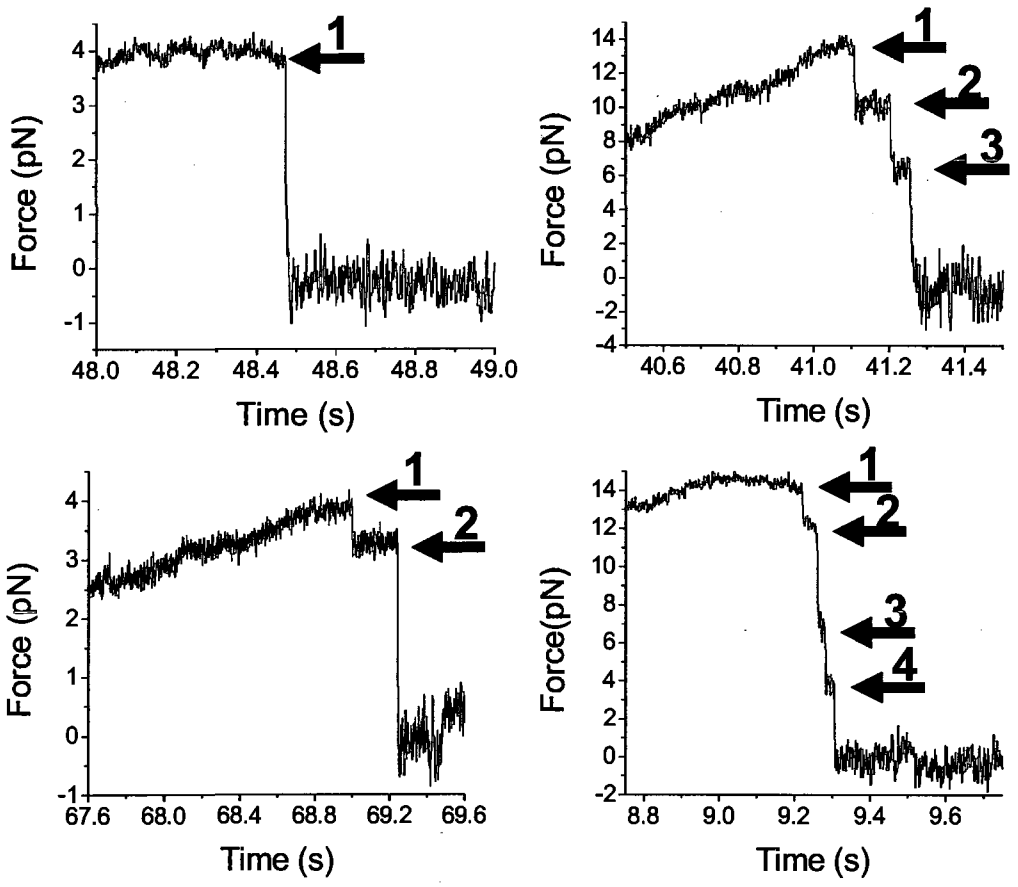

Figure 2.4: Examples of optical trap traces that exhibit one, two, three, and four steps in separate stepwise release events. By eye, one can visualize the trace pause at discrete steps during the bead's descent back to the baseline where the bead reaches the center of the trap.

CHAPTER 3: RESULTS

After data was collected, further analysis was performed. Release events were categorized into one, two, three, four and more release steps separately. Release events numbering five and higher steps were observed, but were in insufficient frequency to attain reasonable statistics ($n < 15$) so they were not analyzed with any scrutiny. For each motor, Eg5 and K560, and each value of stepwise release, one through four, the release force values were compiled into probability histograms (Figs. 3.1, 3.2). The average release force for each was calculated, along with the standard error of the mean (sem), and plots were generated showing the average release force vs. number of motors engaged for both Eg5 and K560 (Table 3.1, Fig. 3.3) (OriginPro 7.5, OriginLab Corp., Northampton, MA). Assuming that motors added linearly to the release force of the bead, one might naively attempt to fit the data to a line. However, plotting these graphs and applying a linear function to the data, weighted by the mean variances with an intercept of 0 pN, lead to reduced chi-squared values of ~87 for Eg5 and ~170 for K560 fits. These large values imply the simple linear model was inadequate to describe the system data. To explain this nonlinearity and more accurately characterize the relationship between release forces and the number of motors, we developed a physical model to describe the system acting on the polystyrene bead. The trapping force we have already described as a linear spring by stating that the force it applies to the bead is described as $\mathbf{F}_t = -\kappa \mathbf{d}_t$, where κ is the trap stiffness in pN/nm and $\mathbf{d}_t$ is the distance from the bead center to the trap center. Yet, motors also exert forces on the bead as they are anchored to the axoneme track. The motor proteins, as well as the linkages from the protein to the bead, have a finite rigidity. Therefore, we will also model the linkage between the motor

and the bead as a linear spring with stiffness k. Its corresponding force on the bead is $\mathbf{F}_m = -k\mathbf{d}_m$, where $\mathbf{d}_m$ is the distance from the motor-axoneme binding site to the attachment site on the bead. A cartoon of this model for two motors engaged in transporting a bead out of the trap is displayed in figure 3.4.

3.1 Spring Model

For our model, we do assume that the force for the motors' release from the axoneme is linear with the number of engaged motors. This model is used to describe the release force of beads in previous works [24, 25], but, as mentioned earlier, the measured release forces for beads in this experiment do not follow a simple linear relationship. The important thing to note is that the experiment does not directly measure the release force on the motors; it measures the release force on the bead. Optical traps are only capable of measuring the force that the trapping laser applies to the bead at the point of release. What we wish to measure is the force applied to the motor/axoneme binding at the point of release. There are more forces in the system than just the trap. Engaged motors also apply forces to the bead, and eachother, which must be taken into account when modeling the measured data. Another assumption we make is that the motor dissociates from the axoneme as it is attempting to take a forward step. Due to the hand-over-hand stepping nature of kinesin motors [18] (Fig. 1.2) at the moment of stepping only one of the motor heads is bound to the axoneme. It is at this point when the leading motor, in a multiple motor system, is also under the most amount of stress, as we will show in the following calculations. Not only is there a rearward force due to the trap, but also from other anchored motors which have not taken a step and are now stretched due to the

displacement of the bead. Here, we will expand upon this concept in the multiple-motor system as one motor takes a single step.

Before a step has been taken the force balancing equation takes the following form:

$$0 = F = -\kappa d_t + k\sum_{i}^{N} d_{mi}$$

N is the number of motors that are actively attaching the bead to the axoneme. After one motor takes one step, displacing its center of mass by a distance of s, we see that the magnitude of the distance the bead has moved, Δd_t, is:

$$\Delta d_t = \frac{s}{N + \frac{\kappa}{k}}$$

and the magnitude of force added on the stepping motor due to it and the bead's change in position is:

$$\Delta F_{m1} = k(s - \Delta d_t)$$

If the motor is only loosely coupled to the bead, i.e. if k is significantly small, then this portion of rearward tension is negligible. That is to say, the bulk of the rearward pull is due to the trapping force, not the other anchored motors. This effect of an insignificant stiffness constant is assumed, perhaps incorrectly, in previous works observing multiple motor transport [24, 25]. In these cases, the measured release force is assumed to be linear with the number of motors engaged; two motors will release at twice the force of one. However, as will become apparent in the work presented here, if this motor/linkage constant, k, is sufficiently large, it will have a measurable effects on the rearward force. We must add this as a correction factor to our release force measurement.

The equation we now fit our measurements to in order to find the actual release force per motor is:

$$F_e = f_r N - k(s - \Delta d_t)$$

where F_e is the release force measured in the optical trapping experiment and f_r is the actual release force of a single motor which we will report here. Here $f_r N$ is the linear portion describing how multiple motors, N, add to the release force. We believe this linear modeling is valid for two reasons. One, it has been previously shown that the stepping rate for kinesin motors significantly decreases with increasing rearward load [62]. This infers that if there is an unequal distribution of load between two or more motors engaged in transport, then the stepping rate of the motors under higher load slows down. This allows time for trailing motors to catch up. This mechanism self corrects for differences in load bearing and drives the system towards a linear distribution at the release point. Secondly, release events of unequal force distribution are discriminated out in our analysis. For instance, in the two motor transport model where one motor is under significantly higher load then the other, the leading motor reaches its release point first. The position trace of the bead will show a release of one motor with the trace dropping sharply to a point, but not to the zero baseline. The second motor, still engaged, will not yet have reached its release force and will continue processing and transporting the bead until it has done so. The trace will resume rising again from this new position to reflect this. These traces are disregarded because they do not fit the profile of a stepwise release. Valid release events must continue all the way to the zero baseline. Hence, we are confident in describing the release force at the motor-axoneme region with the linear term, $f_r N$.

The remaining, nonlinear portion of the equation is the correction that accounts for a motor attempting to take a step forward, succumbing to the added strain of the trap and other motors not advancing, and then releasing from the axoneme all in a time scale shorter than the temporal resolution of the experiment. The step size of an individual motor, s, we assume to be 8.3 nm from previous measurements [28], and due to the nature of our analysis we can determine N for each release event, leaving only two unknowns to be determined; the release force per motor, f_r, and the characteristic stiffness constant, k, for the protein and linkage system.

The points were fit with our model (OriginPro 7.5), weighted by the standard error of the mean (sem), and produced Eg5 values of $k = 1.07 \pm 0.06$ pN/nm and $f_r = 4.71 \pm 0.11$ pN. Experiments and fits with K560 produced $k = 1.16 \pm 0.05$ pN/nm and $f_r = 5.36 \pm 0.07$ pN. Data plots along with the fits are shown in figure 3.5. Corresponding reduced chi-squared values for the fits were 4.7 for Eg5 and 0.37 for K560. OrginPro's fitting algorithms were able to determine that these release force values were statistically different with ~97% degree of confidence. This was an F-Test analysis. It calculated the sum of squared differences (*SSR*) between the fit and the data. Then, replacing the fit parameter (f_r in this case) value with that to be compared to (i.e. replacing $f_r = 4.71$ with $f_r = 5.36$), it repeated a least squares fitting with the remaining parameter, k, and arrived at a new sum of squared differences, *SSR(p)*. Using the equation:

$$SSR(p) = SSR(1 + \frac{F}{DOF})$$

it solved for a value F. DOF is the degrees of freedom for the system, the number of points fitted minus the number of fitting parameters (4 – 2 = 2). Finally, the value F was

compared in an *F*-distribution table to find the corresponding confidence interval, $F = F(confidence, 1, DOF)$. The *confidence* value, in this case, was the reported 97%.

3.2 Control Analysis

When observing multiple release events, it is possible to mistakenly characterize events with an improper motor number because the release step count does not necessarily correspond with the number of motors engaged. A release event with few steps has the potential to come from a larger motor number release if some of the release steps were missed due to insufficient time resolution. To check our potential for this form of error we calculated the probability of *N* motors binding to the axoneme given the geometry of the experiment. We model the bead as a sphere with a radius of 600 nm, the axoneme as a cylinder of radius 80 nm [63], and the motor plus linkage to bead (biotinylated antibody and streptavidin) having a length of 50 nm [64-66]. The probability of *N* motors on the sphere being geometrically able to bind to the axoneme was derived assuming an equal distribution of motors around the bead and that the number of motors within a certain area followed a binomial distribution. Cartoon depictions of the geometry are shown in figure 3.6. Determining the potential for motor engagement required a surface integral taking the form of:

$$\int_{\phi_L}^{\phi_M}\int_{0}^{\theta_M(\phi)} R^2 \sin(\phi)\, d\theta\, d\phi$$

where R is the radius of the polystyrene sphere (600 nm) and $\theta_M(\phi)$, ϕ_L, and ϕ_M are limits derived from the geometries using both the law of sines and the law of cosines.

Chemical binding stoichiometry must also be considered in this calculation, since not all motors in the mixture will be bound to the beads. The exact ratio was determined by the dissociation constants, k_d, governing the bonding of protein to the microsphere. k_d characterizes the chemical reaction:

$$A + B \leftrightarrow AB$$

by relating the concentrations of the reactants and product in the steady-state.

$$k_d = \frac{[A][B]}{[AB]}$$

where $[A]$, $[B]$ and $[AB]$ are the concentrations of the reactants A and B, and the product AB. The streptavidin/biotin interaction is extremely strong with a dissociation constant of approximately 4×10^{-14} M^{-1} [57] so we can safely assume that a negligible amount of biotin binding cites on the streptavidin coating the sphere are without a biotinylated anti-histidine antibody. For histidine-antibody binding we used a k_d of approximately 4×10^{-8} M^{-1}, within the reported range of the antibody/tag interaction (personal communication with QIAGEN, Valencia, CA). From personal communications with the Sperotech company, we know there were approximately 4180 streptavidins per bead (personal communication with Spherotech), four biotin binding sites per streptavidin, and two histidine tag binding sites per antibody. With this information, we attained an average of ~80 motors per bead for the 1:2,000 bead to motor mixing ratio. The calculations were preformed in Mathematica 6.0 for Students (Wolfram Research Inc., Champaign, IL) with a copy of the full worksheet in appendix A.5. Using 80 motors per bead, we calculated the probability of N number of motors being bound to the axoneme at the time of release, for $N = 1, 2, 3$ or 4, and compare them to the portion of release events that occurred in N steps from the experimental data. Given that the issue of larger values of N

motors in a release event mistakenly measured as lower N values has the highest probability of occurring at the largest motor concentration, the calculated probabilities were compared to the measured percentages of the 1:2,000 bead to motor mixing ratios. The comparison between the theoretical and experimental binding is shown in Table 3.2. The strong agreement between measurement and calculation reassures us that very few step release events are missed due to inadequate time resolution.

It should be noted that there is a large range of values the antibody dissociation constant could take. Since the value is unmeasured by the AbD Serotech company or the author, the actual bead to motor ratio is not definitive. So, as an added measure of precaution against this possible misrepresentation of data, release events taken and analyzed as single step releases were gathered only from the samples containing the lowest concentration of motors, a bead to motor mixing ratio of 1:20. Events for two step releases were not taken from the highest motor mixing ratio, 1:2,000, samples in the compilation of average release force histograms (Figs. 3.1, 3.2). This concentration screening ensures that the reported number of motors engaged in a release event is not an underestimate.

Conversely, release events have the potential to be characterized as having more motors engaged than there are. A multiple step release might occur if a single motor dissociates from the axoneme but then quickly rebinds, within the relaxation period of the bead returning to the trap center. It may remain for a brief period and then release again allowing the bead to subsequently reach the trap focus. This scenario would be counted as a two motor event when, in actuality, only one motor was engaged. To determine the

probability of this occurring, we measured the average time between a release event and a subsequent reengagement of the bead to the axoneme, the "rebinding time."

First, the time it took for a bead to travel from the point of motor release to within one standard deviation of the baseline was measured for 100 single step release events. The average for this relaxation time was 15.0 ms. Rebinding times were measured from the beginning of single step releases to the next point at which the bead traveled beyond a baseline standard deviation from the trap center if it continued on to a distance of at least two standard deviations. Histograms of rebinding times fit well to an exponential decay and the average times were taken from the fits (Figs. 3.7, 3.8). Comparing this to the average relaxation time of the bead (15.0 ms) we determined the probability that a motor rebinds immediately after release falsely creating a stepwise release event. The measured rebinding rates and corresponding probabilities of a motor reattachment during the relaxation period for all six samples are listed in Table 3.3. We note that the average rebinding rate is slow enough that the probability of a motor reengaging after dissociation but before the bead has returned to center is fairly insignificant, ~2 - 4%. This assures us that we are indeed seeing multiple motor stepwise release events and properly classifying them as such.

3.3 Figures

Figure 3.1

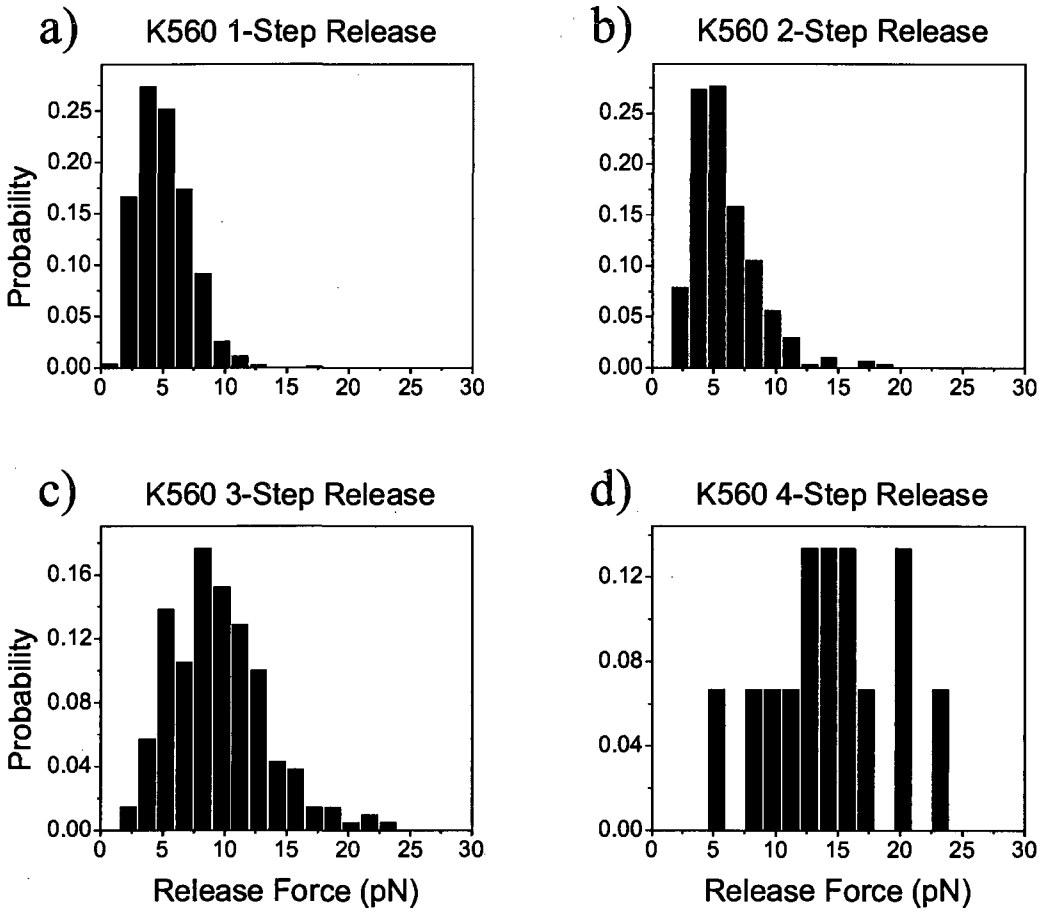

Figure 3.1: Probability histograms of release forces for K560 for a given: a) one step, b) two steps, c) three steps or d) four steps in the release event.

Figure 3.2

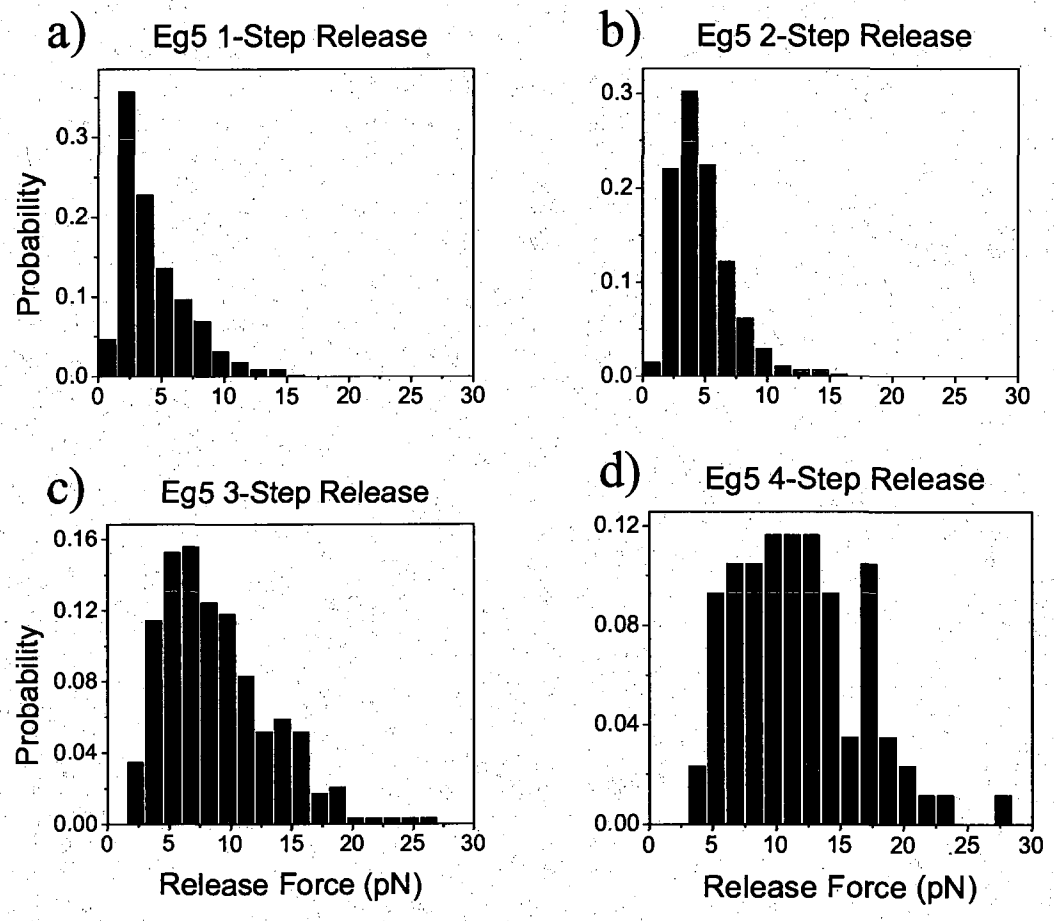

Figure 3.2: Probability histograms of release forces for Eg5 for a given: a) one step, b) two steps, c) three steps or d) four steps in the release event.

Table 3.1

Steps	K560 Release Force (pN)	Eg5 Release Force (pN)
1	5.04 ± 0.07	4.36 ± 0.11
2	5.81 ± 0.15	4.73 ± 0.11
3	9.43 ± 0.27	8.90 ± 0.25
4	15.43 ± 1.60	11.77 ± 0.52

Table 3.1: Values for K560 and Eg5 average release force given the number of steps in the release event. Errors reported are standard error of the mean (sem).

Figure 3.3

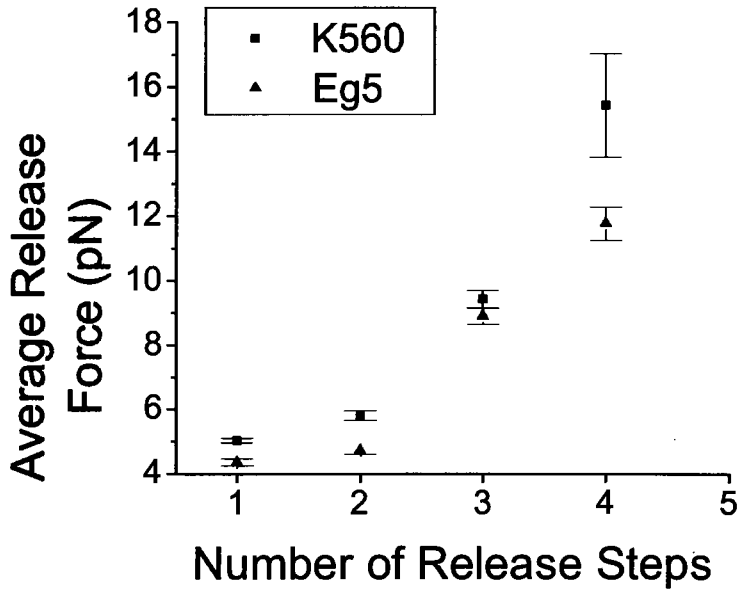

Figure 3.3: Graph of the average release force for K560 (squares) and Eg5 (triangles) versus the number of steps in the release event. Error bars represent the sem.

Figure 3.4

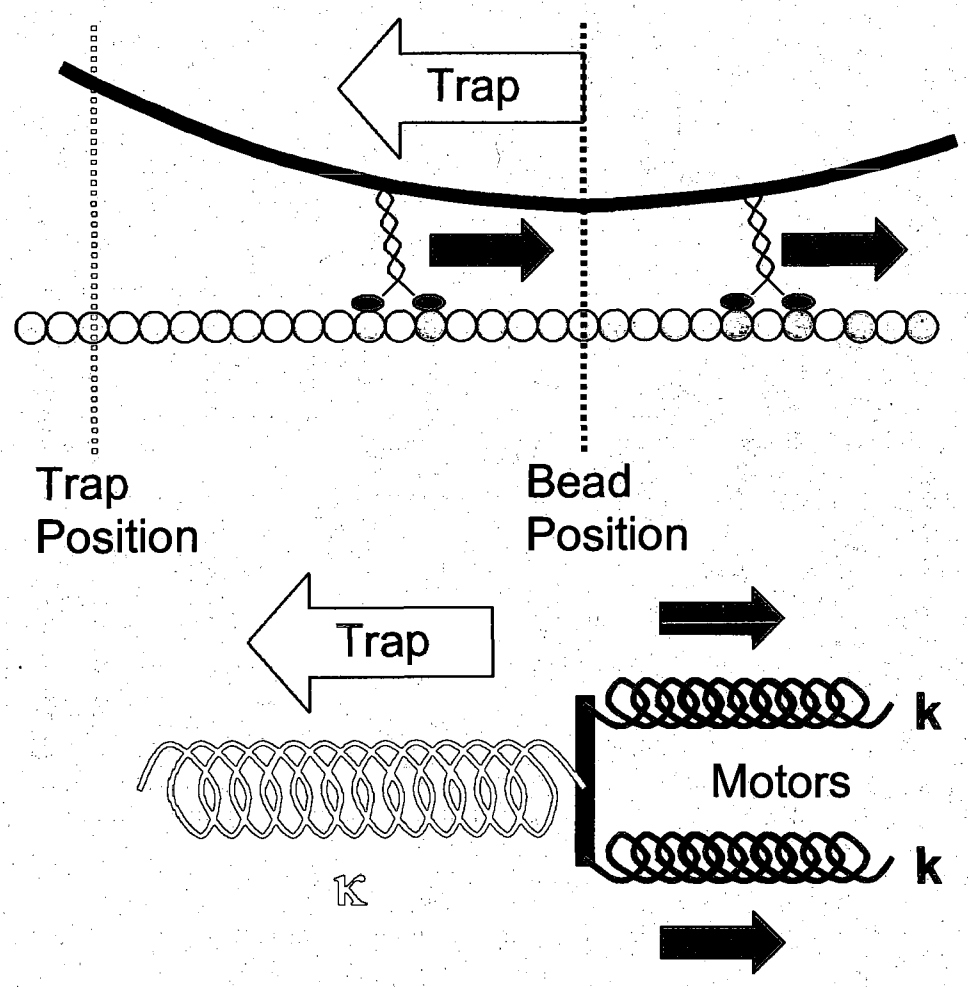

Figure 3.4: Spring model for multiple motor transport of a bead in an optical trap. The bead is displaced to the right of the optical trap by transport of the two motors. The trap can be modeled as an extended spring pulling the bead back to the left with a spring constant κ. The motors are also modeled as springs pulling the bead to the right with spring constants k. At any given instance between stepping the bead is at rest and the forces applied on the bead by the trap and motors must cancel one another.

Figure 3.5

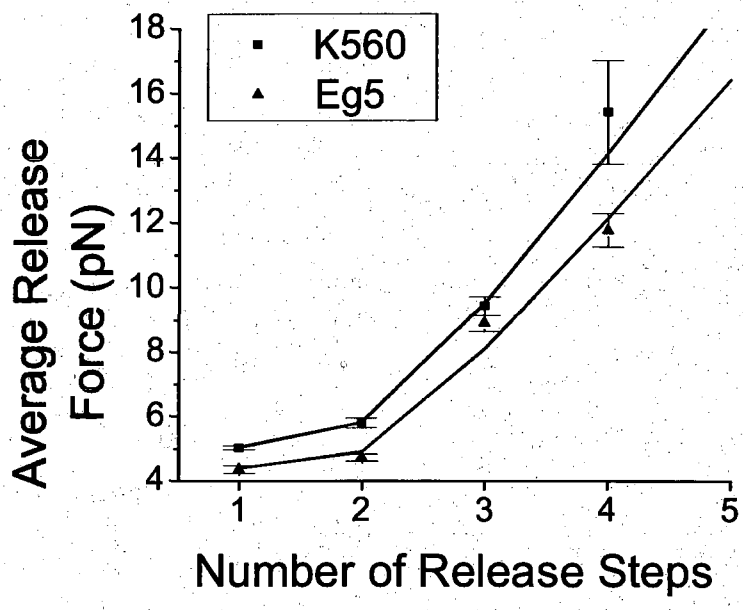

Figure 3.5: Graph of the average release force for K560 (squares) and Eg5 (triangles) versus the number of steps in the release event along with fits generated from the motor spring model. Error bars represent the sem.

Figure 3.6

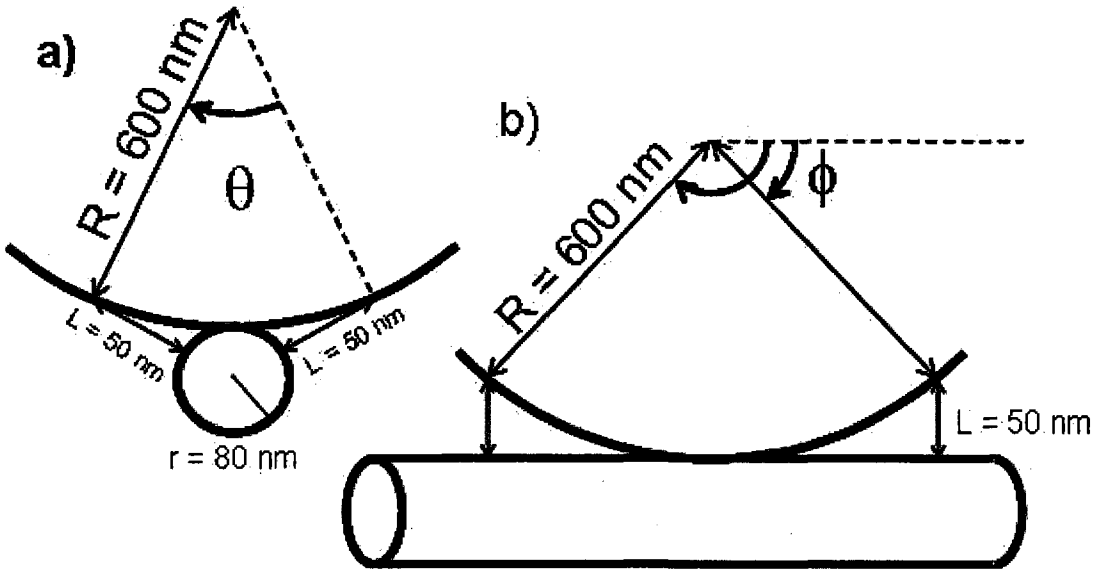

Figure 3.6: Geometry of bead-bound motor engagement onto an axoneme system. The amount of surface area on the bead that allows the possibility of motor engagement on an axoneme was determined by the theoretical steric hindrances depicted here. a) A view of the system looking along the axoneme axis. The bead, radius 600 nm, is above the axoneme, 80 nm radius, and the limits for angle θ are determined by these distances and the limiting length of the motor plus biotin-streptavidin-antibody linkage, 50 nm. b) A side view of the same system displaying how the limits for angle ϕ are determined from the radius of the bead and the motor plus linkage length.

Table 3.2

Steps	Theory	Eg5	K560
1	0.47	0.44	0.53
2	0.32	0.35	0.29
3	0.14	0.14	0.13
4	0.05	0.05	0.04

Table 3.2: Probabilities of observing *N* number of steps within a release event assuming a bead to motor mixing ratio of 1:2,000 and a histidine anti-histidine antibody dissociation constant of 4×10^{-8} M^{-1}. Theoretical calculations are based on assuming simple geometries for a bead and axoneme, known motor and linkage length, and a Poisson distribution of motors within a given bead surface area (Fig 3.6). Experimental probabilities for both motors were derived from the number of recorded events that exhibited *N* steps within the release event divided by the total number of events recorded.

Figure 3.7

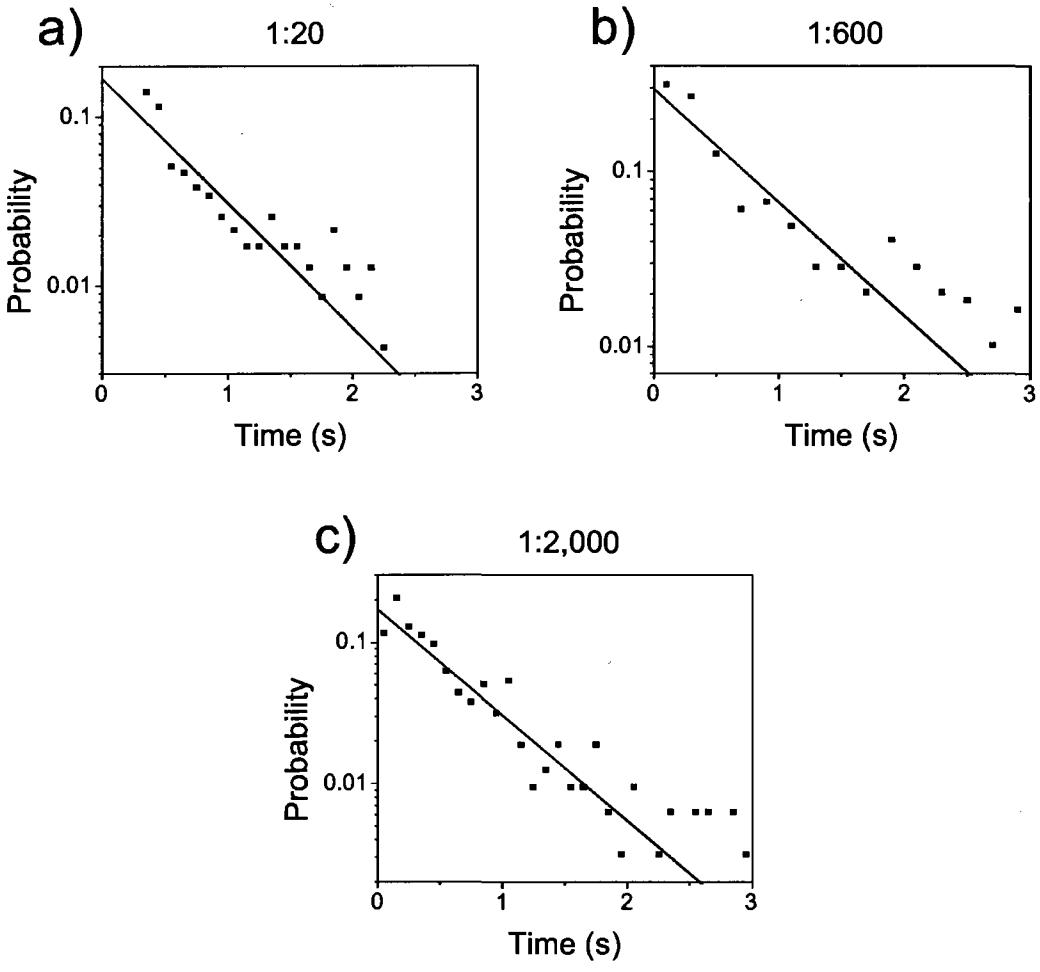

Figure 3.7: Probability histograms of rebinding times for the three concentrations of K560 motors. Histograms were generated by measuring times between the beginning of single-step releases and the subsequent reengagement of the bead with the axoneme. Fits shown here are single exponential decays producing the average characteristic rebinding time reported in table 3.2.

Figure 3.8

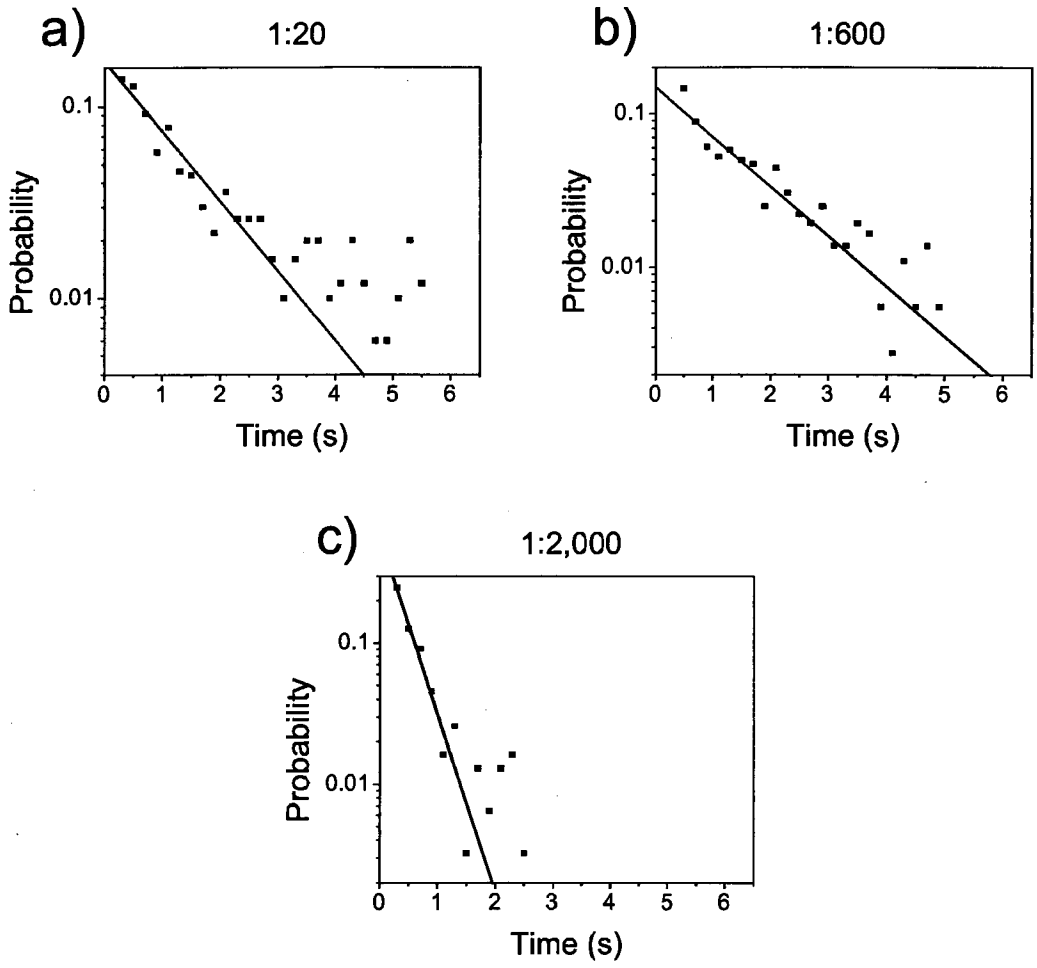

Figure 3.8: Probability histograms of rebinding times for the three concentrations of Eg5 motors. Histograms were generated by measuring times between the beginning of single-step releases and the subsequent reengagement of the bead with the axoneme. Fits shown here are single-exponential decays producing the average characteristic rebinding time reported in table 3.2.

Table 3.3

BtM	Eg5 (ms)	K560 (ms)
1:20	1483 ± 129 (1.0%)*	586 ± 73 (2.5%)*
1:600	1338 ± 109 (1.1%)*	670 ± 78 (2.2%)*
1:2,000	345 ± 37 (4.3%)*	580 ± 43 (2.6%)*

Table 3.3: Average time in ms for a bead to rebind to the axoneme after a release event occurs given a bead-to-motor ratio (BtM) determined by a single-exponential decay fit to the probability histograms (Figs. 3.7, 3.8). *Percent chance of a motor binding the bead to the axoneme within the average relaxation time it takes a free bead to return to the center of the optical trap (15.0 ms) assuming an exponential distribution with the fitted average.

CHAPTER 4: DISCUSSION

Here we have created an Eg5/kinesin-1 chimera (Fig. 1.6) in order to characterize and compare the force properties of cooperating Eg5 motor domains to those of multiple kinesin-1 transporters by utilizing an optical trapping technique (Figs. 1.4, 1.7, 2.1, 2.2). We applied a unique form of data analysis where we take advantage of stepwise release events, categorizing them into the specific number of motors engaged. We confirmed our analysis is reasonable by; a) calculating the theoretical distribution of motors engaged and comparing it to experimental results (Table 3.2), b) using lower amounts of motor for low numbered release event analysis, and c) calculating the probability that a motor binds to the axoneme within the average relaxation time of the bead following a release (Table 3.3). Assured that our analysis is valid, we measured three force characteristics of Eg5 and kinesin-1: a) the rearward force required to achieve bead release (Table 3.1, Fig. 3.3), b) the stiffness of the motor and protein linkage, and c) the average time for a detached motor to rebind the tubulin track (Table 3.3).

4.1 Release Force and Motor Stiffness

Looking at the fitting results from our release force vs. motor number data (Fig. 3.5) we recognize that the motor/linkage stiffness constant for Eg5, $k = 1.07 \pm 0.06$ pN/nm, is statistically equivalent to that of K560, $k = 1.16 \pm 0.05$ pN/nm. Both constructs are identical from the non-helical portion of the protein to the C-terminal histidine tag and the linkage continuing to the bead is also identical; so we conclude that

the region of Eg5 near the N-terminal microtubule binding end differs very little in structural rigidity from kinesin-1.

However, we find that the release force per motor for Eg5, 4.71 ± 0.11 pN, is significantly less than that of K560, 5.36 ± 0.07 pN, with ~97% level of confidence. It is reasonable to suggest that a transport motor like kinesin-1 might require a stronger attachment to microtubules than a cross-linking motor such as Eg5. A transporter shuttling cargo through a mammalian cell is working within a highly viscoelastic cytoplasm and extremely crowded conditions [67]. Also, it is postulated that intracellular cargo is transported by only a small number of molecular motors, between one and five, based on the cryo-electron microscopy studies of vesicle transport [68]. Therefore, a more strongly bound motor, one which can withstand large opposing forces, is presumably more likely to be successful in translating its cargo to remote destinations. In contrast, the function and environment of Eg5 is different. During mitosis, Eg5 concentrations reach ~400nM [69], and the motors are acutely localized on the microtubule spindles, which reach microns in length [70]. Therefore, we presume that Eg5 proteins, attached to a microtubule spanning across the cell, are working in a far greater ratio of motor to cargo than kinesin-1 motors do as transporters. A greater number of motors working together can withstand much greater forces. This makes the number of Eg5 a greater element to successful function, rather than requiring a large release force of a single motor.

The spindle assembly may also use the lower release force of Eg5 as a means of regulating the structure of the microtubule scaffolding. Before anaphase, every chromosome pair must congress at the meridian of the cell spaced specifically between

the two poles [71]. The exact positioning of this division plane is critical for proper reproduction of the cell. Both inhibition and over expression of Eg5 lead to improper spindle formation, postulating that force sensing and balancing are crucial to spindle alignment [72]. This positioning requires communication along the spindles which, we hypothesize, takes the form of force sensing along the axis of the microtubules. The specific release force value of anchoring motors, specifically Eg5, is the kind of force sensing mechanism that could contribute to regulating the length of segregation between poles and organization of the chromosomes in the center.

4.2 Rebinding Times

By measuring the time it takes for an Eg5 to reengage the axoneme after dissociating, we can see the association rate increase as the number of motors engaged increases, as one would expect. However, for K560 it does not (Table 3.3). We find that there is little to no correlation between the concentration of K560 attached to the bead and the rebinding time, since it appears to remain constant at ~600 ms despite a change in bead-to-motor ratio spanning two orders of magnitude, from 1:20 to 1:2,000. This indicates that there is some other interaction that keeps the rate constant despite significant decreases in kinesin-1 concentration. We find a possible explanation to stem from a loose interaction between the truncated form of kinesin-1 and the axoneme present in the unbound state. An attraction which keeps the motor close to the track after dissociation would allow the motor to reengage more easily and possibly mask out any concentration dependence in our rebinding measurements. This is true as long as the interaction between the axoneme and motor is stronger than the translational or rotational

diffusion-forces of the motor or bead. Eliminating the diffusive component of association rate is equivalent to eliminating the rate's concentration dependence. It has been shown that other molecular motors, MCAK, KIF1A and dynein, exhibit one-dimensional diffusion along microtubules. This is evidence of an attracted, yet unbound, state with microtubules [73-77]. 1-D diffusion along tubulin tracks has been shown for Eg5 [78], but, to the authors' knowledge, the results presented here are the first indication that such an interaction may exist for conventional kinesin-1. It should be noted that the presence of a correlation between Eg5 concentration and axoneme association rate is not proof of the absence of the unbound interaction. The interaction may be strong enough to aid in Eg5 association, yet not strong enough to completely eliminate concentration dependence at this level. Further studies at more numerous concentrations could determine the rate equations for the association reactions to determine if there is a concentration independent aspect to them. Our experiments cannot properly characterize these interactions, but can imply that they exist for K560 on a relevant scale at the concentrations presented here. We also conclude that this interaction is localized to the head region of the protein. Due to the construction of our constructs, a coiled-coil domain interaction would be present to the same degree in each motor.

CHAPTER 5: CONCLUSION

We have successfully created an active Eg5/K560 chimera, capable of processively transporting cargo, with the goal of studying the motor domain of Eg5 and comparing it directly to that of kinesin-1. We observe a stepwise release of beads transported by multiple motors within an optical trap providing us with the exact number of proteins engaged in transport. Release events stemming from the disassociation of up to four motors were analyzed providing force characteristics of multiple Eg5 and kinesin-1 motility. The motor stiffness between the motor domains are comparable (1.07 ± 0.06 pN/nm for the motor plus linkage for Eg5 and 1.16 ± 0.05 pN/nm for K560). The force required to dissociate the bead from the axoneme increased with motor number with a value of 4.71 ± 0.11 pN per Eg5 motor and 5.36 ± 0.07 pN per K560 characterizing the linear portion of our release force model. Finally, in our experiments we discover that the time required for K560 to reengage with the axoneme after a release event is independent of motor concentration on the bead (Table 3.3). This differs from the results for Eg5 where we see an increase in the rebinding rate as the motor concentration increases. This result may be evidence of a concentration independent interaction between the kinesin-1 motor domain and axonemes that is not present, or at least not as prevalent, for Eg5 proteins.

5.1 Future Works

Here we have measured and discussed release forces for beads transported by up to four motors. However, Eg5 has the potential to operate at an even higher motor to

cargo ratio in the mitotic spindle. So, can we measure release forces under these conditions? The answer is "Yes." This may be undertaken by a few different methods. A simple extension of the experiments described here would be to take the dimeric Eg5 motor proteins and attach them to polystyrene beads of a larger diameter. This would allow more motors to come in contact with the axoneme because of the increased radius of curvature. Presumably, motors can decorate the surface of the larger bead with the same density. Motors separated by the same distance along the surface of the bead will not be distanced as much from the axoneme due to the curvature of the sphere. This would allow more motors to transport the bead despite maintaining the same surface density.

However, this increased bead diameter study is not likely to get results in the range of mitotic activity. To do so is possible for Eg5, but requires another experiment, such as a combination of microtubule gliding and optical trapping. Native, tetrameric Eg5 has been shown to promote microtubule cross-linking and subsequent gliding [32, 35]. In this proposed experiment, two heads of Eg5 walk along one microtubule that is adhered to the sample chamber surface, while the other two heads walk along a microtubule that is unbound from the surface. As both halves of Eg5 process towards the positive end of each microtubule, the two tubulin filaments will either remain approximately stationary to one another if parallel, or, if they happen to be anti-parallel, the unbound microtubule will move and glide along the axis of the other (Fig. 5.1). Within a single sample, one would witness approximately half of the gliding events in the parallel state and half in the anti-parallel state. It is on the later population which one might conduct this study. By attaching a bead to the free floating microtubules one

attains a handle for the optical trap to make measurements. This attachment can be preformed by polymerizing the microtubules with biotinylated tubulin (#T333, Cytoskeleton Inc., Denver, CO) and mixing them with streptavidin coated polystyrene beads. The optical trap would capture the bead as the Eg5 motors attempt to transport it along the axis of the microtubule. At a certain point, the release force will be reached and the bead-microtubule complex will release and return to the trap center. One could perform this at varying Eg5 concentrations to get a sense of the force dependence on motor number. If stepwise release occurs under these conditions, then one could count the number of motors engaged directly. Alternatively, one has the possibility of counting the motors individually by means of fluorescent techniques such as FIONA [79] or SHRIMP [80] that rely on fitting the distribution of photons emitting from one or numerous fluorophores projected onto a CCD camera. This requires simultaneous trapping and imaging of the sample.

Native Eg5 DNA could be mutated to insert a green fluorescent protein (GFP) sequence so that when the DNA was incorporated into live cells, the cells would produce Eg5 that was fluorescently labeled with GFP. Blue photons, near 488 nm in wavelength, will be absorbed by GFP which will then emit green photons, around 509 nm in wavelength [81]. These green photons can then be selectively singled out with an emission filter (HQ520/50 Chroma) and projected onto a camera for the purposes of localizing the GFP. This would allow the user to observe an image and directly count the number of Eg5 motors along the microtubules using a fluorescence localization technique. This would be an upper limit on the number of motors engaged and not a direct measurement since the image merely proves localization of a motor on one of the

microtubules, not necessarily its active cross-linking between the two. However, by varying the concentrations and proper modeling of motor engagement, one can still arrive at reasonable estimations for release forces at high motor number. This would be as close to mitotic conditions ever achieved in an *in vitro* study. As an aside, one might instead label the Eg5 proteins with any from a number of commercial dyes providing a more robust marker for fluorescence localization studies.

5.3 Figures

Figure 5.1

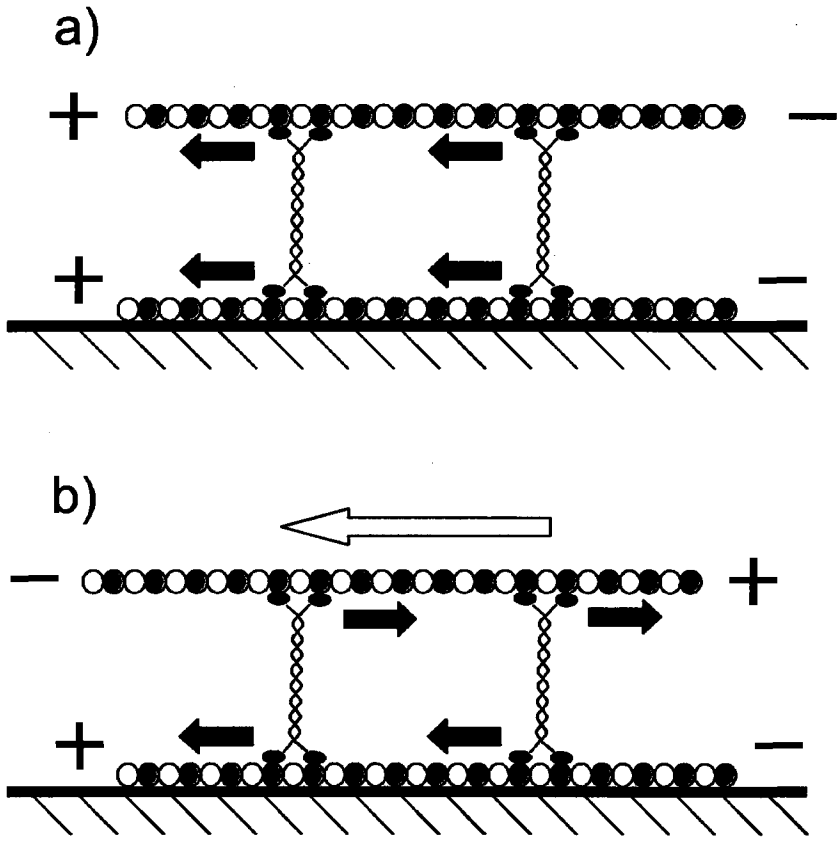

Figure 5.1: Eg5 motors crosslinking microtubules, one of which is bound to the sample surface, and processing along both simultaneously. a) The crosslinked microtubules are parallel. Eg5 motors heads process towards the plus end of each microtubule, but the unbound microtubule does not show motion with respect to the surface bound microtubule. b) The crosslinked microtubules are anti-parallel. Eg5 motors heads process towards the plus end of each microtubule, and the unbound microtubule is transported leftward with respect to the surface bound microtubule.

REFERENCES

1. Alberts, B., et al. 1994. Molecular Biology of the Cell, 3rd ed. Garland Publishing, Inc., New York, NY. 1294.

2. Sancar, A. and M.-s. Tang. 1993. Nucleotide Excision Repair. *Photochemistry and Photobiology*. 57:905-921.

3. Vale, R.D. 1987. Intracellular Transport Using Microtubule-Based Motors. *Annual Review of Cell Biology*. 3:347.

4. Wanka, F. and E.J.J. Van Zoelen. 2003. Force Generation by Cellular Motors. *Cellular & Molecular Biology Letters*. 8:1017-1033.

5. Wilson, A.K., et al. 1992. The role of myosin I and II in cell motility. *Cancer and Metastasis Reviews*. 11:79-91.

6. Hirokawa, N. 1996. Organelle transport along microtubules -- the role of KIFs. *Trends in Cell Biology*. 6:135-141.

7. Hirokawa, N. 1998. Kinesin and Dynein Superfamily Proteins and the Mechanism of Organelle Transport. *Science*. 279:519-526.

8. Hirokawa, N., Y. Noda, and Y. Okada. 1998. Kinesin and dynein superfamily proteins in organelle transport and cell division. *Current Opinion in Cell Biology*. 10:60-73.

9. Sharp, D.J., G.C. Rogers, and J.M. Scholey. 2000. Cytoplasmic dynein is required for poleward chromosome movement during mitosis in Drosophila embryos. *Nat Cell Biol*. 2:922-930.

10. Vale, R.D. and R.J. Fletterick. 1997. The Design Plan of Kinesin Motors. *Annual Review of Cell and Developmental Biology*. 13:745.

11. Hirokawa, N., et al. 1989. Submolecular domains of bovine brain kinesin identified by electron microscopy and monoclonal antibody decoration. *Cell*. 56:867-878.

12. Woehlke, G., et al. 1997. Microtubule Interaction Site of the Kinesin Motor. *Cell*. 90:207-216.

13. Gelfand, V.I. and A.D. Bershadsky. 1991. Microtubule Dynamics: Mechanism, Regulation, and Function. *Annual Review of Cell Biology*. 7:93.

14. Miki, H., Y. Okada, and N. Hirokawa. 2005. Analysis of the kinesin superfamily: insights into structure and function. *Trends in Cell Biology*. 15:467-476.

15. Holzinger, A. and U. Lütz-Meindl. 2002. Kinesin-Like Proteins are Involved in Postmitotic Nuclear Migration of the Unicellular Gree Alga Micrasterias Denticulata. *Cell Biology International*. 26:689-697.

16. Brady, S.T., K.K. Pfister, and G.S. Bloom. 1990. A monoclonal antibody against kinesin inhibits both anterograde and retrograde fast axonal transport in squid axoplasm. *Proceedings of the National Academy of Sciences of the United States of America*. 87:1061-1065.

17. Diefenbach, R.J., et al. 1998. The C-Terminal Region of the Stalk Domain of Ubiquitous Human Kinesin Heavy Chain Contains the Binding Site for Kinesin Light Chain&#x2020. *Biochemistry*. 37:16663-16670.

18. Yildiz, A., et al. 2004. Kinesin Walks Hand-Over-Hand. *Science*. 303:676-678.

19. Schnitzer, M.J., K. Visscher, and S.M. Block. 2000. Force production by single kinesin motors. *Nat Cell Biol*. 2:718-723.

20. Block, S.M., L.S.B. Goldstein, and B.J. Schnapp. 1990. Bead movement by single kinesin molecules studied with optical tweezers. *Nature*. 348:348-352.

21. Cai, D., K.J. Verhey, and E. Meyhöfer. 2007. Tracking Single Kinesin Molecules in the Cytoplasm of Mammalian Cells. *Biophysical Journal*. 92:4137-4144.

22. Kural, C., et al. 2005. Kinesin and Dynein Move a Peroxisome in Vivo: A Tug-of-War or Coordinated Movement? *Science*. 308:1469-1472.

23. Vale, R.D., et al. 1996. Direct observation of single kinesin molecules moving along microtubules. *Nature*. 380:451-453.

24. Shubeita, G.T., et al. 2008. Consequences of Motor Copy Number on the Intracellular Transport of Kinesin-1-Driven Lipid Droplets. *Cell*. 135:1098-1107.

25. Vershinin, M., et al. 2007. Multiple-motor based transport and its regulation by Tau. *Proceedings of the National Academy of Sciences*. 104:87-92.

26. Kojima, H., et al. 1997. Mechanics of single kinesin molecules measured by optical trapping nanometry. *Biophysical Journal*. 73:2012-2022.

27. Kuo, S.C. and M.P. Sheetz. 1993. Force of single kinesin molecules measured with optical tweezers. *Science*. 260:232-234.

28. Svoboda, K., et al. 1993. Direct observation of kinesin stepping by optical trapping interferometry. *Nature*. 365:721-727.

29. Visscher, K., M.J. Schnitzer, and S.M. Block. 1999. Single kinesin molecules studied with a molecular force clamp. *Nature*. 400:184-189.

30. Cole, D.G., et al. 1994. A "slow" homotetrameric kinesin-related motor protein purified from Drosophila embryos. *J. Biol. Chem.* 269:22913-22916.

31. Kashina, A.S:, G.C. Rogers, and J.M. Scholey. 1997. The bimC family of kinesins: essential bipolar mitotic motors driving centrosome separation. *Biochimica et Biophysica Acta (BBA) - Molecular Cell Research.* 1357:257-271.

32. Kapitein, L.C., et al. 2005. The bipolar mitotic kinesin Eg5 moves on both microtubules that it crosslinks. *Nature.* 435:114-118.

33. Epstein, H. and J.M. Scholey. 1992. Kinesins in the spindle: an update. *Trends in Cell Biology.* 2:315-318.

34. Kashlna, A.S., et al. 1996. A bipolar kinesin. *Nature.* 379:270-272.

35. Sharp, D.J., et al. 1999. Antagonistic microtubule-sliding motors position mitotic centrosomes in Drosophila early embryos. *Nat Cell Biol.* 1:51-54.

36. Blangy, A., et al. 1995. Phosphorylation by p34cdc2 regulates spindle association of human Eg5, a kinesin-related motor essential for bipolar spindle formation in vivo. *Cell.* 83:1159-1169.

37. Heck, M.M., et al. 1993. The kinesin-like protein KLP61F is essential for mitosis in Drosophila. *J. Cell Biol.* 123:665-679.

38. Bergnes, G., K. Brejc, and L. Belmont. 2005. Mitotic Kinesins: Prospects for Antimitotic Drug Discovery. *Current Topics in Medicinal Chemistry.* 5:127-145.

39. Duhl, D.M. and P.A. Renhowe. 2005. Inhibitors of kinesin motor proteins--research and clinical progress. *Curr Opin Drug Discov Devel.* 8:431-436.

40. Hildebrandt, E.R. and M.A. Hoyt. 2000. Mitotic motors in Saccharomyces cerevisiae. *Biochimica et Biophysica Acta (BBA) - Molecular Cell Research.* 1496:99-116.

41. Walczak, C.E., et al. 1998. A model for the proposed roles of different microtubule-based motor proteins in establishing spindle bipolarity. *Current Biology.* 8:903-913.

42. Greenleaf, W.J., M.T. Woodside, and S.M. Block. 2007. High-Resolution, Single-Molecule Measurements of Biomolecular Motion. *Annual Review of Biophysics and Biomolecular Structure.* 36:171.

43. Mehta, A.D., K.A. Pullen, and J.A. Spudich. 1998. Single molecule biochemistry using optical tweezers. *FEBS Letters.* 430:23-27.

44. Valentine, M.T., et al. 2006. Individual dimers of the mitotic kinesin motor Eg5 step processively and support substantial loads in vitro. *Nat Cell Biol.* 8:470-476.

45. deCastro, M.J., et al. 2000. Working strokes by single molecules of the kinesin-related microtubule motor ncd. *Nat Cell Biol.* 2:724-729.

46. Block, S.M., *Optical tweezers: a new tool for biophysics*, in *Noninvasive Techniques in Cell Biology*, F.K. Foskett and S. Grinstein, Editors. 1990, Wiley-Liss: New York. p. 375–402.

47. Saleh, B.E.A. and M.C. Teich. 1991. Fundamentals of Photonics. John Wiley & Sons, Inc., New York. 966.

48. Korneev, M., S. Lakämper, and C. Schmidt. 2007. Load-dependent release limits the processive stepping of the tetrameric Eg5 motor. *European Biophysics Journal.* 36:675-681.

49. Desai, A., et al. 1999. Kin I Kinesins Are Microtubule-Destabilizing Enzymes. *Cell.* 96:69-78.

50. Friedman, D.S. and R.D. Vale. 1999. Single-molecule analysis of kinesin motility reveals regulation by the cargo-binding tail domain. *Nat Cell Biol.* 1:293-297.

51. Yardimci, H., et al. 2008. The mitotic kinesin CENP-E is a processive transport motor. *Proceedings of the National Academy of Sciences.* 105:6016-6021.

52. Yonekura, H., et al. 2006. Mechanism of tail-mediated inhibition of kinesin activities studied using synthetic peptides. *Biochemical and Biophysical Research Communications.* 343:420-427.

53. Coppin, C.M., et al. 1997. The load dependence of kinesin's mechanical cycle. *Proceedings of the National Academy of Sciences of the United States of America.* 94:8539-8544.

54. Hall, K., et al. 1996. Kinesin force generation measured using a centrifuge microscope sperm-gliding motility assay. *Biophysical Journal.* 71:3467-3476.

55. Case, R.B., et al. 1997. The Directional Preference of Kinesin Motors Is Specified by an Element outside of the Motor Catalytic Domain. *Cell.* 90:959-966.

56. Pierce, D.W. and R.D. Vale. 1998. Assaying processive movement of kinesin by fluorescence microscopy. *Methods Enzymol.* 298:154-171.

57. Green, M.N., M. Wilchek, and E.A. Bayer, *Avidin and streptavidin*, in *Methods in Enzymology.* 1990, Academic Press. p. 51-67.

58. Aitken, C.E., R.A. Marshall, and J.D. Puglisi. 2008. An Oxygen Scavenging System for Improvement of Dye Stability in Single-Molecule Fluorescence Experiments. *Biophysical Journal.* 94:1826-1835.

59. Appleyard, D.C., et al. 2007. Optical trapping for undergraduates. *American Journal of Physics*. 75:5-14.

60. Visscher, K., S.P. Gross, and S.M. Block. 1996. Construction of multiple-beam optical traps with nanometer-resolution position sensing. *Selected Topics in Quantum Electronics, IEEE Journal of*. 2:1066-1076.

61. Svoboda, K. and S.M. Block. 1994. Biological Applications of Optical Forces. *Annual Review of Biophysics and Biomolecular Structure*. 23:247.

62. Block, S.M., et al. 2003. Probing the kinesin reaction cycle with a 2D optical force clamp. *Proceedings of the National Academy of Sciences of the United States of America*. 100:2351-2356.

63. Sakakibara, H.M., et al. 2004. Diameter Oscillation of Axonemes in Sea-Urchin Sperm Flagella. *Biophysical Journal*. 86:346-352.

64. Darst, S.A., et al. 1991. Two-dimensional crystals of streptavidin on biotinylated lipid layers and their interactions with biotinylated macromolecules. *Biophysical Journal*. 59:387-396.

65. Edelman, G.M. 1991. Antibody Structure and Molecular Immunology. *Scandinavian Journal of Immunology*. 34:4-22.

66. Kerssemakers, J., et al. 2006. The distance that kinesin-1 holds its cargo from the microtubule surface measured by fluorescence interference contrast microscopy. *Proceedings of the National Academy of Sciences*. 103:15812-15817.

67. Guigas, G., C. Kalla, and M. Weiss. 2007. Probing the Nanoscale Viscoelasticity of Intracellular Fluids in Living Cells. *Biophysical Journal*. 93:316-323.

68. Miller, R.H. and R.J. Lasek. 1985. Cross-bridges mediate anterograde and retrograde vesicle transport along microtubules in squid axoplasm. *Journal of Cell Biology*. 101:2181-2193.

69. Kapoor, T.M. and T.J. Mitchison. 2001. Eg5 is static in bipolar spindles relative to tubulin: evidence for a static spindle matrix. *J. Cell Biol.* 154:1125-1134.

70. Whitehead, C.M., R.J. Winkfein, and J.B. Rattner. 1996. The relationship of HsEg5 and the actin cytoskeleton to centrosome separation. *Cell Motility and the Cytoskeleton*. 35:298-308.

71. Bajer, A.S. and J. Mole-Bajer. 1972. Spindle dynamics and chromosome movements. International review of cytology, 3. Academic Press, New York.

72. Castillo, A., et al. 2007. Overexpression of Eg5 Causes Genomic Instability and Tumor Formation in Mice. *Cancer Res*. 67:10138-10147.

73. Culver-Hanlon, T.L., et al. 2006. A microtubule-binding domain in dynactin increases dynein processivity by skating along microtubules. *Nat Cell Biol.* 8:264-270.

74. Endow, S.A. and D.S. Barker. 2003. Processive and nonprocessive models of kinesin movement. *Annual Review of Physiology.* 65:161.

75. Helenius, J., et al. 2006. The depolymerizing kinesin MCAK uses lattice diffusion to rapidly target microtubule ends. *Nature.* 441:115-119.

76. Okada, Y. and N. Hirokawa. 2000. Mechanism of the single-headed processivity: Diffusional anchoring between the K-loop of kinesin and the C terminus of tubulin. *Proceedings of the National Academy of Sciences.* 97:640-645.

77. Vale, R.D., D.R. Soll, and I.R. Gibbons. 1989. One-dimensional diffusion of microtubules bound to flagellar dynein. *Cell.* 59:915-925.

78. Kwok, B.H., et al. 2006. Allosteric inhibition of kinesin-5 modulates its processive directional motility. *Nat Chem Biol.* 2:480-485.

79. Yildiz, A., et al. 2003. Myosin V Walks Hand-Over-Hand: Single Fluorophore Imaging with 1.5-nm Localization. *Science.* 300:2061-2065.

80. Gordon, M.P., T. Ha, and P.R. Selvin. 2004. Single-molecule high-resolution imaging with photobleaching. *Proceedings of the National Academy of Sciences of the United States of America.* 101:6462-6465.

81. Heim, R., A.B. Cubitt, and R.Y. Tsien. 1995. Improved green fluorescence. *Nature.* 373:663-664.

APPENDIX: SOFTWARE PROGRAMS

A.1 Trapstiff.m

The following two MATLAB program was used to determine the stiffness of the trap given raw QPD voltage data from an unbound bead captured within the trap. It reads the data, takes a Fourier transform, and fits the power spectrum to a Lorentzian curve as described in section 2.2.2.2.

```
function results = trapstiff(powerfile)
%Derives stiffness and the corner frequency from raw voltage data taken
at
%16,384Hz for 20sec.

%Written by Evan Graves 08/27/08

%   Reference:
%      [1]  Tolic-Norrelykke, Schaffer, Howard, Pavone, Julicher,
%      and Flyvberg "Calibration of Optical Tweezers with Positional
%      Detection in the Back Focal Plane", Review of Scientific
%      Instruments 77, 2006 p. 103101-1 through 11.

%      [2] Neuman and Block, "Optical Trapping." Rev Sci Instrum.
%      2004 Sep;75(9):2787-809.

filenam = powerfile;

%Read in the file
Voltages = dlmread(filenam);

%Rearrange the 20sec data acquisitions, at F Hz, into 20 columns
f = 16384;
Xvolts = zeros(f,20);
Yvolts = zeros(f,20);

for i = 1:20
    for j = 1:f
        Xvolts(j,i) = Voltages(j+f*(i-1),2) ./ Voltages(j+f*(i-1),4);
        Yvolts(j,i) = Voltages(j+f*(i-1),3) ./ Voltages(j+f*(i-1),4);
    end
end

%Create Power Spectrum data from the voltage data
```

```
FFTx = fft(Xvolts)/f;
FFTy = fft(Yvolts)/f;

PowerX = abs(FFTx(1:f/2+1,1:20)).^2*2;
PowerY = abs(FFTy(1:f/2+1,1:20)).^2*2;

%Average all the columns into one power spectrum
AvPowX = mean(PowerX,2);
AvPowY = mean(PowerY,2);

%The first value in the FFT data is just the sum of all the points.
%Delete it
AvPowX(1) = [];
AvPowY(1) = [];

%Transform the spectra into position space instead of voltage space
%assuming Beta in the X direction is 918nm/[V] and in the Y
%direction 1059nm/[V] based on 09-28-08 calibrations.
AvPowXp = AvPowX.*918^2;
AvPowYp = AvPowY.*1059^2;

%Fit the spectra to Lorentzians and attain the corner frequency,
%FC, and trap stiffness, KAPPA.
%Initial guesses for FC are 1,000Hz and for KAPPA are 0.1pN/nm.

F = (1:f/2)';
AvPowXn = AvPowXp(1:f/2);
AvPowYn = AvPowYp(1:f/2);
FitX = nlinfit(F,AvPowXn,@powerstiff,[1000,.1]');
FitY = nlinfit(F,AvPowYn,@powerstiff,[1000,.1]');

%Plot the power spectrum along with the fits for the X and Y axes.
Xfit = powerstiff(FitX,F); %Fit line for X
Yfit = powerstiff(FitY,F); %Fit line for Y

clf;
subplot(2,1,1);
loglog(F, AvPowXn);
hold on
loglog(F, Xfit, 'Color', [1 0 0]);
subplot(2,1,2)
loglog(F, AvPowYn);
hold on
loglog(F, Yfit, 'Color', [1 0 0]);

%The results are printed as FC and KAPPA for the X direction
%followed by FC and KAPPA for the Y direction.
digits(4);
results = sym([FitX,FitY],'d');

%Calculate the trap stiffness using the equipartition theorem

Xpos = Xvolts.*918;
Ypos = Yvolts.*1059;
Xvar = var(Xpos);
```

```
Yvar = var(Ypos);
eqStiffX = 4.0/mean(Xvar)
eqStiffY = 4.0/mean(Yvar)
```

A.2 Powerstiff.m

This is the Lorentzian function called in the fitting section of the program above.

```
function lorentz = powerstiff(fitvalues,x)

%Lorentzian fit to a Power Spectrum in terms of stiffness and the
corner frequency.
%   LORENTZ = POWERSTIFF(FITVALUES,X) gives the predicted values of the
%   optical trap stiffness, KAPPA, and corner frequency, FC
%   given a power spectrum X.

%   Reference:
%      [1]  Tolic-Norrelykke, Schaffer, Howard, Pavone, Julicher,
%      and Flyvberg "Calibration of Optical Tweezers with Positional
%      Detection in the Back Focal Plane", Review of Scientific
%      Instruments 77, 2006 p. 103101-1 through 11.

%      [2] Neuman and Block, "Optical Trapping." Rev Sci Instrum.
%      2004 Sep;75(9):2787-809.

fc = fitvalues(1);
kappa = fitvalues(2);

lorentz = 2*4.0/pi()/kappa./(fc+x.^2./fc);
```

A.3 Stepfall.m

This function was used to analyze raw QPD voltage data from trapping experiments. The software creates a projection of the bead's motion along the axoneme and allows the user to select stepwise release events. It then records the measured release force and the number of steps in the event and writes them all to a .csv file for future analysis.

```
function [Results] = stepfall(Inputfile)
```

```
%STEPFALL will read in a .txt file of QPD voltage, allow the user to
click
%around peak areas to be analysed, then output a file containing those
%peaks in pN.  INPUTFILE is the path and name of the file surrounded by
%single quotes (').

%Written by Evan T. Graves 07/01/08
%modified 09/28/08

%Read in the data file in .txt format.
Data = dlmread(Inputfile);
L = length(Data);
Xdata = Data(:,5);
Ydata = Data(:,6);

%Fit the data to a line y = mx + b and create the unit vector along it.
Lfit = polyfit(Xdata, Ydata, 1);
m = Lfit(1);
b = Lfit(2);
X1 = min(Xdata);
X2 = max(Xdata);
Y1 = m*X1 + b;
Y2 = m*X2 + b;

ux = sqrt(1 / (1 + m^2));
uy = ux * m;
uv = [ux; uy];

%Project the position onto the line fit and convert unitless,
normalized
%voltage into pN.  Use calibrations from 09/28/08.
BetaX = 918;
BetaY = 1059;
StiffX = 0.0819;
StiffY = 0.0988;

XF = Xdata.*BetaX.*StiffX;
YF = Ydata.*BetaY.*StiffY;

Proj = [XF YF] * uv;

%Smooth the data by averageing with the previous W-1 points.
W = 50;
SProj = Proj;
for i = W:L
    SProj(i,:) = mean(Proj(i-(W-1):i,:));
end

%Plot the smoothed data along with the raw position trace and line fit.
clf;
subplot(2,1,1);
plot(SProj(W:L));
subplot(2,1,2);
plot(Xdata, Ydata);
```

```
hold on
line([X1 X2], [Y1 Y2], 'Color', [1 0 0], 'LineWidth', 3);

%Have the user click on two points that outline the baseline.
BaseX = ginput(2);
BaseLeft = floor(BaseX(1,1)) + W-1;
BaseRight = ceil(BaseX(2,1)) + W-1;
Baseline = mean(Proj(BaseLeft:BaseRight));
SD = std(SProj(BaseLeft:BaseRight));

%Break the projection plot up into N sections and then allow the user
to
%click on points right before detachmet. Average this point with the
%previous NN-1 points to determine the disassociatin peak.
N = 10;
Np = L/N;
NN = 10;
t = 1:Np;
Base = Baseline + zeros(Np,1);
BaseUP = Base + SD;
BaseDWN = Base - SD;
Peaks = zeros(0,5,5);
n = [1 1 1 1 1];

for k = 1:N  %Break up the graph into N pieces to analyse individually.
    clf;
    plot(SProj(Np*(k-1)+1:Np*k));
    hold on
    plot(t,Base,t,BaseUP, ':', t, BaseDWN, ':', 'Color', [1 0 0]);
    PT = ginput(1);  %Click on the peak

    while PT(1) > 0
        Px = floor(PT(1)) + Np*(k-1);
        P = abs(mean(SProj(Px-NN+1:Px)) - Baseline);  %get the peak
value
        St = ginput(1);  %click the next step in the peak release
        Steps = zeros(1,5);  %A max of 5 steps is assumed
        Steps(1) = P;
        l = 2;

        %Allow the user to click on extra steps in the release.
        %After the steps are selected click to the right of the graph
to be
        %finished with the peak and move on to the next.
        while St(1) < Np
            Sx = floor(St(1)) + Np*(k-1);
            S = abs(mean(SProj(Sx-NN+1:Sx)) - Baseline);
            Steps(l) = S;
            St = ginput(1);
            l = l+1;
        end

        NZS = nnz(Steps);  %number of steps (non-zero elements)
        Peaks(n(NZS),:,NZS) = Steps;  %write the peak into the matrix
        n(NZS) = n(NZS) + 1;
```

```
        PT = ginput(1);  %click the next peak or finish by clicking
left
    end
end

%Write the values to .csv files. the number at the end of the filename
%represents the number of steps that occured in the release process.
%Each row within a file is a seperate peak.  The first column is the
peak
%value and the remaining columns contain the values of release steps
InputName = Inputfile(1:length(Inputfile)-4); %take off ".txt"
OutputName1 = [InputName 'peaks1.csv']; %add "peaks.csv" to filename
OutputName2 = [InputName 'peaks2.csv'];
OutputName3 = [InputName 'peaks3.csv'];
OutputName4 = [InputName 'peaks4.csv'];
OutputName5 = [InputName 'peaks5.csv'];

if max(max(Peaks(:,:,1))) > 0
    csvwrite(OutputName1, Peaks(:,1,1));
end
if max(max(Peaks(:,:,2))) > 0
    csvwrite(OutputName2, Peaks(:,1:2,2));
end
if max(max(Peaks(:,:,3))) > 0
    csvwrite(OutputName3, Peaks(:,1:3,3));
end
if max(max(Peaks(:,:,4))) > 0
    csvwrite(OutputName4, Peaks(:,1:4,4));
end
if max(max(Peaks(:,:,5))) > 0
    csvwrite(OutputName5, Peaks(:,1:5,5));
end
```

A.4 Timefall.m

This function was used to analyze raw QPD voltage data from trapping experiments. The software creates a projection of the bead's motion along the axoneme and allows the user to select times in between the beginning of release events and the beginning of bead mobility reengagement, the rebinding times. It then records the rebind times and writes them all to a .csv file for future analysis.

```
function [Results] = timefall(Inputfile)

%TIMEFALL will read in a .txt file of QPD voltage, allow the user to
click
```

```
%the points between a release and a rebinding to determine the time
%inbetween. INPUTFILE is the path and name of the file surrounded by
%single quotes ('). It will then write out all the individual times,
the
%total summed time, the number of spacings, and the average time.

%Written by Evan T. Graves 12/03/08

%Read in the data file in .txt format.
Data = dlmread(Inputfile);
L = length(Data);
Xdata = Data(:,5);
Ydata = Data(:,6);

%Fit the data to a line y = mx + b and create the unit vector along it.
Lfit = polyfit(Xdata, Ydata, 1);
m = Lfit(1);
b = Lfit(2);
X1 = min(Xdata);
X2 = max(Xdata);
Y1 = m*X1 + b;
Y2 = m*X2 + b;

ux = sqrt(1 / (1 + m^2));
uy = ux * m;
uv = [ux; uy];

%Project the position onto the line fit and convert unitless,
normalized
%voltage into pN.  Use calibrations from 09/28/08.
BetaX = 918;
BetaY = 1059;
StiffX = 0.0819;
StiffY = 0.0988;

XF = Xdata.*BetaX.*StiffX;
YF = Ydata.*BetaY.*StiffY;

Proj = [XF YF] * uv;

%Smooth the data by averageing with the previous W-1 points.
W = 50;
SProj = Proj;
for i = W:L
    SProj(i,:) = mean(Proj(i-(W-1):i,:));
end

%Plot the smoothed data along with the raw position trace and line fit.
clf;
subplot(2,1,1);
plot(SProj(W:L));
subplot(2,1,2);
plot(Xdata, Ydata);
hold on
line([X1 X2], [Y1 Y2], 'Color', [1 0 0], 'LineWidth', 3);
```

```
%Have the user click on two points that outline the baseline.
BaseX = ginput(2);
BaseLeft = floor(BaseX(1,1)) + W-1;
BaseRight = ceil(BaseX(2,1)) + W-1;
Baseline = mean(Proj(BaseLeft:BaseRight));
SD = std(Proj(BaseLeft:BaseRight));

%Break the projection plot up into N sections and then allow the user
to
%click on points right after detachmet.
N = 4;
Np = L/N;
t = 1:Np;
Base = Baseline + zeros(Np,1);
BaseUP = Base + SD/2;
BaseDWN = Base - SD/2;
Times = zeros(0,4);
n = 1;

for k = 1:N  %Break up the graph into N pieces to analyse individually.
    clf;
    plot(SProj(Np*(k-1)+1:Np*k));
    hold on
    plot(t,Base,t,BaseUP, ':', t, BaseDWN, ':', 'Color', [1 0 0]);
    PT = ginput(1);  %Click on the first fall

    while PT(1) > 0
        P1 = floor(PT(1));
        PT2 = ginput(1);  %click where the next rebinding rise occurs
        P2 = floor(PT2(1));
        Tim = P2 - P1;  %Calculate the difference between points
        Times(n,1) = Tim;  %Record the time difference in a matrix
        n = n + 1;  %Increase the index of the difference measurement
        PT = ginput(1);  %Click after the next fall or left of axis to
end.
    end
end

Tot = sum(Times);
Num = size(Times);

if Num(1) > 0
    Times(1,2) = Tot(1);
    Times(1,3) = Num(1);
    Times(1,4) = Tot(1)/Num(1);

    %Write the times out in a .csv file
    InputName = Inputfile(1:length(Inputfile)-4); %take off ".txt"
    OutputName = [InputName 'times.csv'];  %add "times.csv"
    csvwrite(OutputName, Times);
end

Results = Num(1);
```

A.5 Steric Hinderance.nb

The following Mathmatica command lines were used in the control analysis outlined in section 3.2 concerning the theoretical estimation of the number of motors attached to a bead that could simultaneously engage the axoneme. Here, the limits for the surface integral over the bead were set according to geometries shown in figure 3.6. The integral is carried out, the estimation of the number motors in that area of the bead is determined and the probability of a release event having one, two, three, or four motors engaged was determined. These values are compared with experimental results in table 3.2.

```
eq1=(R+r)^2+(R*Sin[p])^2-(r+l)^2-2*(R*Sin[p])*(R+r)*Cos[t]

p1=ArcSin[(R-l)/R]

R=600.
r=80.
l=50.

p2=p1+2*(Pi/2-p1)

Tlim=Solve[eq1==0,t]

Tint=Integrate[R^2*Sin[p],{t,t/.Tlim[[1]],t/.Tlim[[2]]}]

Pint=NIntegrate[Tint,{p,p1,p2}]

Prop=Pint/(4*Pi*R^2)

p2000=Prop*80

pp2000[0]=Exp[-p2000]
pp2000[1]=p2000^1*Exp[-p2000]/1!/(1-pp2000[0])
pp2000[2]=p2000^2*Exp[-p2000]/2!/(1-pp2000[0])
pp2000[3]=p2000^3*Exp[-p2000]/3!/(1-pp2000[0])
pp2000[4]=p2000^4*Exp[-p2000]/4!/(1-pp2000[0])
```

CURRICULUM VITAE

EVAN TACLIBON GRAVES

2137 Market St., La Crosse, WI 54601 USA
Tel. (217) 721-1587 * Evan.Graves@Gmail.com

EDUCATION

Ph.D. Physics (Biophysics) 2000 – 2009
University of Illinois, Urbana, IL

M.A. Physics (Biophysics) 2000 – 2002
University of Illinois, Urbana, IL

B.S. Physics and Mathematics (*magna cum laude*) 1996 – 2000
Rose-Hulman Institute of Technology, Terre Haute, IN

PROFESSIONAL EXPERIENCE

University of Illinois, Urbana-Champaign 2001 –
Ph.D. Candidate (Biophysics), Department of Physics present
Thesis Advisor: Dr. Paul R. Selvin

- Conceived, conducted, and analyzed numerous single-molecule research experiments focused on conformational, motility and force characterization of proteins from seven different families of molecular motors (Myosin II, Myosin V, Myosin VI, Myosin IX, Kinesin-1, Eg5, Kar3).
- Personally designed, custom built and rigorously troubleshot laser-implementing optical instrumentation for experimental purposes.
    - Four total-internal-reflection microscopes for multi-colored, fluorescently labeled protein localization and real-time motion tracking.
    - A confocal microscope for fluctuation-correlation spectroscopy and single-pair Förster resonance energy transfer measurements
    - An emission spectrometer with fluorescence spectrum and lifetime analysis capabilities for measuring lanthanide resonance energy transfer.
    - An optical trap apparatus for manipulation, position tracking, and force property characterization of molecular motor coated microspheres.

- Programmed and implemented software pertinent to experimental research
    - Algebraic and statistical modeling of physical and biological systems.
    - Gathering and analysis of large output data files from various photo detectors including APDs, PMTs and video files from CCD cameras.
- Acquired expertise in a broad range of biochemical techniques.
    - DNA: point-mutagenesis, ligation, PCR amplification, bacterial cell transformation, expression, purification and quantization through gel electrophoresis and absorption spectroscopy.
    - Proteins: bacterial cell expression, purification from cells, purification from animal tissue, chemical labeling with fluorescent markers or polystyrene microspheres, quantization through gel electrophoresis and absorption/emission spectroscopy, and functionality characterization through ATPase activity and actin/microtubule gliding assays.
- Complied research results in the form of written publication and dissertation.
- Presented results at Selvin lab meetings, University of Illinois group seminars and the Biophysical Society National Conference.
- Assisted with the completion for successful grant proposals for competitive renewal funding from the National Institute of Health.
- Edited and assessed the worth of journal articles submitted for peer review.

Lab Manager, Selvin Biophysics Lab 2002 – 2006

- Mentored graduate and post-doctoral researchers concerning ongoing projects.
- Supervised daily operations of the Selvin Biophysics Lab.
    - Delegated lab employee work-loads.
    - Supervised lab organization and inventory.
    - Oversaw lab adherence to university and governmental regulations.

Purdue University, West Lafayette, IN

Undergraduate Summer Researcher, Department of Physics 1999

Research Supervisor: Andrew S. Hirsch

- Researched and assembled an electronic circuit for the purpose of measuring and analyzing chaotic properties displayed when harmonically driven.
- Studied and presented characterizations of the chaos displayed.

FELLOWSHIPS, AWARDS, AND HONORS

National Institute of Health Molecular Biophysics Training Grant
University of Illinois Academic Fellowship
National Science Foundation Research Experience for Undergraduates
John W. Rhee Award for Outstanding Senior in Physics
C. Leroy Mason Award for Outstanding Sophomore in Physics
Sigma Pi Sigma, National Physics Honors Society
Pi Mu Epsilon, National Mathematics Honors Society

COMPUTER PROFICIENCIES

MS-Office, MATLAB, Maple, Mathematica, OriginLab, Labview